

K-CORRECTIONS AND FILTER TRANSFORMATIONS IN THE ULTRAVIOLET, OPTICAL, AND NEAR-INFRARED

MICHAEL R. BLANTON¹ AND SAM ROWEIS²

Received 2006 June 7; accepted 2006 October 11

ABSTRACT

Template fits to observed galaxy fluxes allow calculation of K -corrections and conversions among observations of galaxies at various wavelengths. We present a method for creating model-based template sets given a set of heterogeneous photometric and spectroscopic galaxy data. Our technique, nonnegative matrix factorization, is akin to principal component analysis (PCA), except that it is constrained to produce nonnegative templates, it can use a basis set of models (rather than the delta-function basis of PCA), and it naturally handles uncertainties, missing data, and heterogeneous data (including broadband fluxes at various redshifts). The particular implementation we present here is suitable for ultraviolet, optical, and near-infrared observations in the redshift range $0 < z < 1.5$. Since we base our templates on stellar population synthesis models, the results are interpretable in terms of approximate stellar masses and star formation histories. We present templates fitted with this method to data from *Galaxy Evolution Explorer*, Sloan Digital Sky Survey spectroscopy and photometry, the Two Micron All Sky Survey, the Deep Extragalactic Evolutionary Probe, and the Great Observatories Origins Deep Survey. In addition, we present software for using such data to estimate K -corrections.

Key words: galaxies: fundamental parameters — galaxies: photometry — galaxies: statistics

Online material: color figures

1. MOTIVATION

New surveys at low and high redshift have provided us with estimates of galaxy spectral energy distributions (SEDs) for an enormous number of galaxies. When comparing populations of galaxies at different redshifts in these surveys, we need to use comparable measurements of the galaxy SEDs. However, different surveys use different bandpasses, and the rest-frame wavelengths of these bandpasses necessarily vary with redshift. We need to be able to handle this heterogeneity in order to make sensible comparisons among all of these new surveys.

In this paper we present a method for doing so by calculating K -corrections between observed and desired bandpasses. The K -correction between a bandpass R used to observe a galaxy at redshift z and the desired bandpass Q is defined by the equation (Oke & Sandage 1968; Hogg et al. 2002)

$$m_R = M_Q + \text{DM}(z) + K_{QR}(z) - 5 \log h, \quad (1)$$

where $\text{DM}(z) = 25 + 5 \log[d_L/(h^{-1} \text{ Mpc})]$ is the bolometric distance modulus calculated from the luminosity distance d_L , and M_Q is the absolute magnitude. The absolute magnitude is defined as the apparent magnitude an object would have if it were observed 10 pc away, in bandpass Q , at rest. The traditional definition of the K -correction takes $Q = R$. However, we note that in practice many surveys do perform K -corrections from one observed bandpass R to another bandpass Q in the rest frame. This practice is particularly common when dealing with high-redshift observations. In addition to K -corrections, this method also provides an interpretation of the data in terms of a physical model that describes the stellar mass and star formation history of each galaxy.

The method is designed to work well for a wide range of data sets. It uses photometry and spectroscopy of the Sloan Digital

Sky Survey (SDSS; York et al. 2000), the *Galaxy Evolution Explorer* (*GALEx*; Martin et al. 2005) in the ultraviolet, and the Two Micron All Sky Survey (2MASS; Skrutskie et al. 1997) in the near-infrared (NIR). In addition, at higher redshifts we use constraints from the Deep Extragalactic Evolutionary Probe 2 (DEEP2; Davis et al. 2003; Faber et al. 2003) and the Great Observatories Origins Deep Survey (GOODS; Giavalisco et al. 2004). These and other data sets provide a huge set of information about galaxy colors and spectra that we can use to help understand their star formation histories.

We note that some of the algorithmic techniques used here may have applications in other areas of astrophysics. First, nonnegative matrix factorization (NMF; Lee & Seung 2000), and the extensions to it we describe here, is a particularly useful variant of principal component analysis (PCA). Second, the nonnegative least-squares algorithm of Sha et al. (2002) has the virtue of being extremely simple to implement. These methods may find other applications in image analysis, spectroscopic analysis, and model fitting in astrophysics.

We also release the templates in electronic form and an implementation of the methods used to fit the templates to data. This software, `kcorrect v4_1`, is distributed on the World Wide Web.³ It consists of a core C library that performs most of the complex and computationally intensive tasks plus an IDL library that provides a high-level interface. This software is an update of two major earlier releases (v1_16; Blanton et al. 2003b; v3_2). The improvement over the previous version is twofold. First, we have improved the templates such that they successfully fit galaxies in the rest-frame UV, as observed by *GALEx*, DEEP2, and GOODS. Second, because the templates are now completely model-based, the fits have a physical interpretation in terms of a star formation history. The IDL library also has a number of new useful functions.

In § 2 we describe how to find suitable templates, given a set of models and a set of data. We also describe the data and models

¹ Center for Cosmology and Particle Physics, New York University, New York, NY, USA.

² Department of Computer Science, University of Toronto, Toronto, ON, Canada.

³ Available at <http://cosmo.nyu.edu/blanton/kcorrect/>.

used here. In § 3 we show the results: the best-fit templates and how well they fit the data. In § 4 we describe how to convert our results into an estimate of the K -correction. In § 5 we describe the physical interpretation of the templates and of fits to data. In § 6 we present some simplified, linear transformations between various bandpasses. In § 7 we summarize our results. Appendix A describes the NMF algorithm. Appendix B describes the electronic format of our results.

Where necessary, we have assumed cosmological parameters $\Omega_0 = 0.3$, $\Omega_\Lambda = 0.7$, and $H_0 = 100h \text{ km s}^{-1} \text{ Mpc}^{-1}$ (with $h = 1$), unless otherwise noted. All magnitudes are (unless otherwise noted) AB-relative. Except where noted, we always refer to the version of the `kcorrect` software labeled v4_1_4.

2. FINDING THE TEMPLATES

2.1. Overview

From spectroscopic observations we know that galaxy spectra reside in a low-dimensional subspace of all possible spectra. PCA of galaxy spectra, introduced by Connolly et al. (1995) and applied many times since then, demonstrates that most of the variance in the distribution of galaxies in spectral space can be explained using a few templates. This means that, in the linear space of all possible spectra, galaxies exist in only a small subspace. Therefore, even with very heterogeneous data, we should be able to determine the properties of this subspace.

Here we present an approach to combining heterogeneous data in order to determine the properties of the subspace of galaxy spectra. Rather than taking the model-free approach used by PCA, we here restrict the space of possible spectra to those predicted from the high-resolution stellar population synthesis model of Bruzual & Charlot (2003) and the nebular emission-line models of Kewley et al. (2001). This approach both constrains the problem appropriately and yields a natural theoretical interpretation of the results in terms of star formation histories. Generalizing this approach to use other models of emission from stars and gas is straightforward.

In a nutshell, our algorithm does the following. Given the observations (and uncertainties of those observations) available for each galaxy, it finds the nonnegative linear combination of N template star formation histories that best predict those observations in the χ^2 sense. Given the entire set of galaxy observations available, it also fits for the N template star formation histories. The technical name for this algorithm is nonnegative matrix factorization (Lee & Seung 1999, 2000), and we describe it in detail in Appendix A. Note that this problem is not the same as the well-known nonnegative least-squares problem, which would fit for the best-fit nonnegative linear combination of templates but not for the form of the templates themselves.

This approach is similar to PCA in that it finds the small spectral subspace in which galaxies exist and can in some ways be thought of as “nonnegative PCA.” However, our method has several advantages over the standard PCA approach. First, the results yield, along with a subspace in the space of all possible spectra, a natural interpretation, which is the corresponding subspace in the space of all possible star formation histories. Second, it naturally handles data uncertainties and missing data, which allows it to ignore variation that is due purely to statistical errors. PCA, by contrast, does not use any information about the known uncertainties and is therefore left free to assign templates to express variations that are purely due to errors. Third, it handles the complications of observing galaxy spectra photometrically using broadband filters of galaxies at varying redshifts, whereas

standard PCA requires a constant grid of observations in rest-frame wavelength space.

In the following subsections we introduce the basis set of models we use here (§ 2.2), the data to which we fit (§ 2.3), and how we combine the two to set up the NMF problem (§ 2.4). In Appendix A we describe how to actually solve the NMF problem.

2.2. The Models

We begin with a basis set of 485 spectral templates. Of these, 450 are a set of instantaneous bursts from Bruzual & Charlot (2003) using the Chabrier (2003) stellar initial mass function and the Padova 1994 isochrones. We use all six metallicities (mass fractions of elements heavier than He of $Z = 0.0001, 0.0004, 0.004, 0.008, 0.02$, and 0.05). For each metallicity we select 25 ages (between 1 Myr and 13.75 Gyr, spaced almost logarithmically in age). We smooth each template to 300 km s^{-1} velocity dispersion (we smooth the SDSS spectra in the training set to the same resolution).

There are limitations to all stellar population synthesis libraries, and our results are therefore restricted to be at best as good as our input models. There are some well-known areas of uncertainty in the stellar population models in the UV and IR. In the UV, old populations sometimes contain extreme horizontal branch stars that have lost their envelopes and are thus extremely hot, and that dominate the flux at $\lambda \sim 1500 \text{ \AA}$. There is certainly no physical model that predicts when this happens and no consensus about how these stars should be accounted for in isochrone synthesis (that is, what fraction of stars undergo this phase as a function of mass and metallicity). While the models of Bruzual & Charlot (2003) do contain post-asymptotic giant branch (post-AGB) stars and planetary nebula phases that provide far-UV flux in old populations, they do not contain extreme horizontal branch stars or other candidates that might provide more of the UV excess seen in elliptical galaxies (Greggio & Renzini 1990; Brown et al. 2000).

In the NIR, the spectra of thermally pulsating asymptotic giant branch (TP-AGB) stars may dominate the flux in certain intermediate-age populations (0.5–2 Gyr). Maraston (2005) showed that including TP-AGB spectra based on nearby TP-AGB stars, rather than on the models of Vassiliadis & Wood (1993) used by Bruzual & Charlot (2003), produces significantly higher flux in the NIR at intermediate ages. Thus, the choices for AGB and post-AGB evolution we make here by using the models of Bruzual & Charlot (2003) are not definitive, but we do not address these controversies here, and they remain an uncertainty in the physical interpretation of galaxy fluxes. We do note that for low-redshift galaxies our results from Bruzual & Charlot (2003) do explain most galaxies’ colors (although see below for our discussion of the high-redshift GOODS sample).

For each age and metallicity we make three choices of dust model: (1) no dust extinction; (2) $\tau_V = 3$ dust with Milky Way-type extinction (as input into the models of Witt & Gordon [2000] with a “homogeneous” distribution and “shell” geometry); and (3) $\tau_V = 3$ dust with Small Magellanic Cloud-type extinction (from the same models).

The remaining 35 templates are from MAPPINGS-III (Kewley et al. 2001) models of emission from ionized gas. We choose the predictions for an 8 Myr old continuous star formation history with five possible metallicities ($Z = 0.001, 0.004, 0.008, 0.02$, and 0.04) and seven possible ionization parameters ($q = 5 \times 10^6, 10^7, 2 \times 10^7, 4 \times 10^7, 8 \times 10^7, 1.5 \times 10^8$, and $3 \times 10^8 \text{ cm s}^{-1}$). We take the spectra (given as a set of delta functions) and smooth them to 300 km s^{-1} velocity dispersion. The one alteration we

make to all of these templates is to remove Ly α , because it is generally much larger than observed in real galaxies. We warn readers that galaxies exhibit many individual variations in equivalent widths of emission lines; our final set of five templates does not have any hope of following these variations in detail.

Let us refer to these 485 basis templates as $M_j(\lambda)$, expressed in units of ergs s $^{-1}$ Å $^{-1}$. We seek to reduce this full basis space to a subspace in which galaxies actually exist. In particular, we seek five templates $F_i(\lambda)$ built from nonnegative combinations of the original basis set of N templates,

$$F_i(\lambda) = \sum_j b_{ij} M_j(\lambda), \quad (2)$$

in units of ergs s $^{-1}$ Å $^{-1}$. In principle, we could seek any number of templates; from our experiments, we have found that five turns out to be a number large enough to explain the data we use here. For each galaxy k we want our model $\hat{F}_k(\lambda)$ for their spectrum to be a nonnegative sum of these five templates:

$$\hat{F}_k(\lambda) = \sum_i a_{ki} F_i(\lambda). \quad (3)$$

2.3. The Data

The training set consists of

1. SDSS spectroscopic data in the observed range 3800 Å < λ < 9000 Å, for 400 luminous red galaxies (LRGs) with $0.15 < z < 0.5$ (Eisenstein et al. 2001) and 1600 main-sample galaxies with $0.001 < z < 0.4$ (Strauss et al. 2002).
2. SDSS photometric data on an independent set of LRGs (*griz* photometry only) and main-sample galaxies (using the full *ugriz* photometry) in the same redshift ranges. We use 2000 LRGs and 7000 main-sample galaxies. For these galaxies we include 2MASS JHK_s extended source catalog data (Jarrett et al. 2000) where available.

3. *GALEx* Data Release 1 (DR1) far-UV (~ 1500 Å) and near-UV (~ 2300 Å) photometry for main-sample SDSS galaxies with redshifts and *ugriz* photometry (4000 galaxies; Martin et al. 2005).

4. The *BRI* photometry for high-redshift galaxies in the DEEP2 DR1 release with $0.6 < z < 1.5$ (4000 galaxies; Davis et al. 2003; Faber et al. 2003).

5. The *BVizJHK_s* photometry for GOODS galaxies with $0.5 < z < 2$ (1000 galaxies; Giavalisco et al. 2004).

The SDSS, 2MASS, and *GALEx* galaxies were selected from and the matches were obtained by the New York University Value-Added Galaxy Catalog (Blanton et al. 2005).

The SDSS data processing consists of astrometry (Pier et al. 2003); source identification, deblending, and photometry (Lupton et al. 2001); photometricity determination (Hogg et al. 2001); calibration (Fukugita et al. 1996; Smith et al. 2002); spectroscopic target selection (Eisenstein et al. 2001; Strauss et al. 2002; Richards et al. 2002); spectroscopic fiber placement (Blanton et al. 2003a); and spectroscopic data reduction. We recalibrated our photometry using the “ubercalibration” procedure described in Blanton et al. (2005). Descriptions of these pipelines also exist in Stoughton et al. (2002). An automated pipeline called `idlspec2d`⁴ (in this case v4_9) measures the redshifts and classifies the reduced spectra (D. Schlegel et al. 2007, in preparation). We use the Petrosian magnitudes for the SDSS data (except where noted below for the LRG-only sample). Using the measured velocity dispersions of the spectra from `idlspec2d`, we further smooth

all spectra in the training sets such that each spectrum has a dispersion of 300 km s $^{-1}$, to ensure consistency of resolution among all the spectra and models.

For the *GALEx* and GOODS data we use “auto” magnitudes, which are the Kron-like magnitudes from SExtractor (Bertin & Arnouts 1996). For 2MASS we use the extrapolated magnitudes from the Extended Source Catalog (Jarrett et al. 2000).

Note that there are 20 different broadband photometric filters listed above (B in DEEP2 is different than the B used by GOODS). The `kcorrect` product described in § 7 contains a tabulation of the response functions for all of these filters.

2.4. Comparing Data and Models

The data consist of spectra and broadband photometric measurements of galaxies at a number of redshifts, and we have to relate the models to these measurements.

For the spectra, we take the observed spectrum $f_k(\lambda)$ (in ergs cm $^{-2}$ s $^{-1}$ Å $^{-1}$) of each galaxy k at redshift z [corresponding to a luminosity distance $d_L(z)$ in cm; see Hogg 1999] and calculate the rest-frame luminosity per unit wavelength:

$$F_k(\lambda) = f_k[\lambda(1+z)](1+z)(4\pi d_L^2). \quad (4)$$

That is, the spectrum is shifted due to the redshift, while the integral of the numerator over wavelength (the total luminosity) is constant with redshift, and the total flux is related to the total luminosity by the inverse-square law. In addition, we smooth each spectrum by such an amount that, given its estimated velocity dispersion, its total velocity dispersion after smoothing is 300 km s $^{-1}$ (there are a small number of galaxies with larger velocity dispersions, which we leave unchanged).

Note that if we discretize the spectra to wavelengths λ_l , the relationship between the predicted SED for a galaxy k and the basis set M_{jl} becomes simply

$$\hat{F}_{kl} = \sum_{ij} a_{ki} b_{ij} M_{jl}. \quad (5)$$

If one has a spectrum for a galaxy the expression for the contribution to χ^2 from each wavelength λ_l in the spectrum is then quite simple:

$$\begin{aligned} \chi_{kl}^2 &= \left[\frac{F_k(\lambda_l) - \hat{F}_k(\lambda_l)}{\sigma_k^2(\lambda_l)} \right]^2 \\ &= \left[\frac{F_k(\lambda_l) - \sum_{ij} a_{ki} b_{ij} M_{jl}}{\sigma_k^2(\lambda_l)} \right]^2. \end{aligned} \quad (6)$$

Comparing observed broadband flux measurements is a bit more complicated, because it is a projection of the spectrum onto the broadband filter p at the observed redshift z . Instead of adjusting the observed fluxes as we could so easily do for the spectra above, for the photometry we express the models in terms of predicted broadband fluxes at each redshift.

Here we define a unit of “maggies” μ_p , which for a given object k is the ratio of the measured signal due to that object relative to the signal from a standard source. AB maggies are relative to the signal from an AB standard source. For example, if we transform our spectral energy density basis function $M_j(\lambda)$ to a flux density $m_j(\lambda)$, we can calculate the contribution of that basis function to the predicted maggies as

$$\mu_{jp} = \frac{\int_0^\infty d\lambda \lambda R_p(\lambda) m_j(\lambda)}{\int_0^\infty d\lambda \lambda R_p(\lambda) f_{AB}(\lambda)}. \quad (7)$$

⁴ Available on the World Wide Web at <http://skymaps.info>.

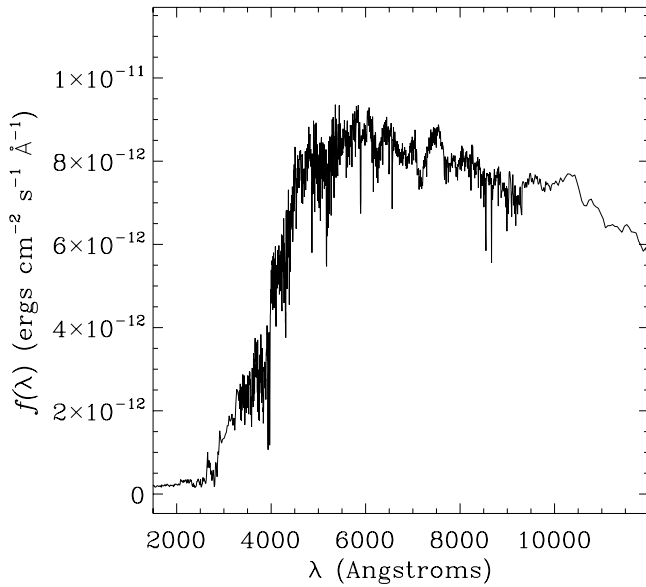


FIG. 1.—Best-fit LRG spectral template in the rest frame. Normalization is for a $1 M_{\odot}$ galaxy located 10 pc away, or, equivalently, a $10^{12} M_{\odot}$ galaxy located 10 Mpc away.

Here, the response function $R_p(\lambda)$ is proportional to the contribution to the detector signal of a photon with wavelength λ entering Earth's atmosphere (or entering the telescope for a space telescope). The AB standard source is $f_{AB}(\lambda) d\lambda = f_{AB}(\nu) d\nu$ and $f_{AB}(\nu) = 3631 \text{ Jy} = 3.631 \times 10^{-20} \text{ ergs s}^{-1} \text{ cm}^{-2} \text{ Hz}^{-1}$. Of course, magnitudes μ are related to magnitudes m as

$$m = -2.5 \log \mu, \quad (8)$$

such that the AB standard source would (if it existed) have $\mu = 1$ and $m = 0$ for all bandpasses.

In this context it is worth noting that many authors (e.g., Bessell 1990) tabulate the contribution to the detector signal per *unit of energy* in photons of wavelength λ instead of per *photon* with wavelength λ . We refer here to the former quantity as $R'_p(\lambda)$, although in the literature it is often referred to without a prime (and without any explicit definition!). Clearly $R_p(\lambda) \propto R'_p(\lambda)/\lambda$, since at a fixed response per unit energy there is a higher response per photon at higher photon frequencies. With this substitution, one can re-express equation (7) appropriately in terms of $R'_p(\lambda)$. Generally, although not universally, authors tabulate $R'_p(\lambda)$ for bandpasses whose standards were originally calibrated using energy-counting devices rather than photon-counting devices. However, from the point of view of the analysis of the observations it is irrelevant what the devices used for the standards and the observations are, as long as one calculates $R_p(\lambda)$ and uses equation (7).

The prediction for the broadband fluxes from equation (7) is only for a specific redshift z . It turns out to simplify our mathematics to calculate the projection of each basis function j onto each filter p for a grid of redshifts (in this case spaced by 0.005 between redshifts 0 and 2). Thus, below we take p to index all the filters at all such redshifts.

Just as before, we can now write down the relationship between the predicted broadband flux and the basis set μ_{jp} , in the bandpass and redshift corresponding to the index p , for a galaxy k :

$$\hat{\mu}_{kp} = \sum_{ij} a_{ki} b_{ij} \eta_{jp}. \quad (9)$$

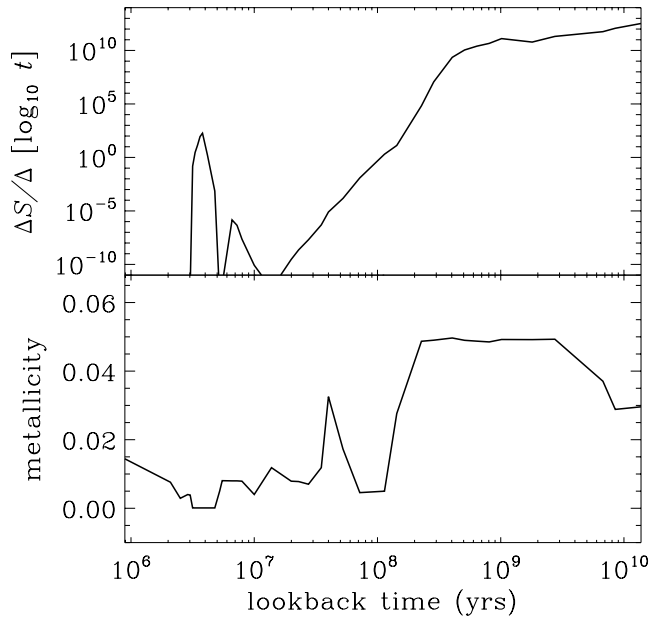


FIG. 2.—Star formation history corresponding to LRG spectral template of Fig. 1. Top: Number of stars normalized for a $10^{12} M_{\odot}$ galaxy. Almost all of the stars are formed in the first couple of billion years; note that the recent "spike" represents a tiny fraction ($\sim 10^{-8}$) of the total number of stars. Bottom: Mean metallicity of the population as a function of time. Note that the details of these functions are rather poorly constrained.

The contribution to the total χ^2 of a broadband flux is therefore just

$$\chi^2_{kp} = \left(\frac{\mu_{kp} - \hat{\mu}_{kp}}{\sigma_{kp}} \right)^2 = \left(\frac{\mu_{kp} - \sum_{ij} a_{ki} b_{ij} \eta_{jp}}{\sigma_{kp}^2} \right)^2. \quad (10)$$

For a given galaxy we do not have every filter, and we only have an observation of each filter at a single redshift. We pick the closest redshift on the redshift grid, use the measured filters at that redshift for our expression of χ^2 , and set $1/\sigma_{kp}^2 = 0$ for the rest of the values of the index p so that we zero-weight those predictions.

The matrices η_{jp} (related to the broadband fluxes) and M_{jl} (related to the spectra) are totally fixed; we combine them into a single matrix M_{jn} and the indices p and l into a single index n to handle both the broadband fluxes and spectra simultaneously. We can similarly combine our observations μ_{kp} and $F_k(\lambda_l)$ and their uncertainties σ_{kp} and $\sigma_k(\lambda_l)$ into vectors x_{kn} and σ_{kn} . Then we can combine equations (6) and (10) into a single equation:

$$\chi^2 = \sum_{kn} \left(\frac{x_{kn} - \sum_{ij} a_{ki} b_{ij} M_{jn}}{\sigma_{kn}} \right)^2. \quad (11)$$

We can use NMF to iterate to the nonnegative a_{ki} and b_{ij} that locally minimize equation (11). The basic method is implemented in a public piece of code named `NMF_SPARSE` in the `idlutils` distribution of IDL utilities.⁵ As the name implies, our implementation takes advantage of the fact that many of the matrix operations are on very sparse matrices (e.g., for each galaxy with photometric data there are no spectroscopic data points and only photometric data at a single redshift).

As we describe in Appendix A, the NMF problem is not convex; that is, there are multiple local minima. Our method finds

⁵ Available at <http://skymaps.info>.

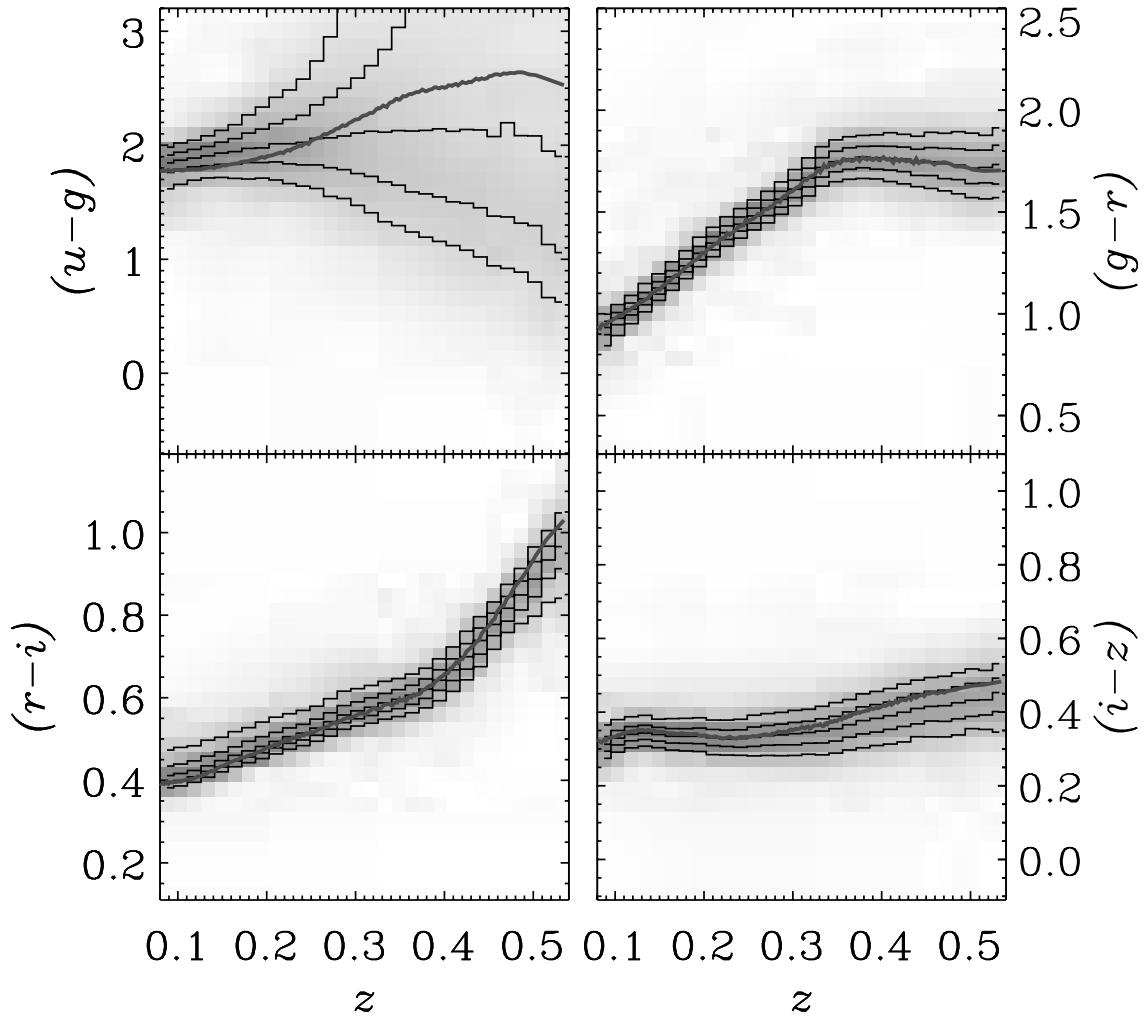


FIG. 3.—SDSS colors of LRGs as a function of redshift. The gray scale is the conditional distribution of color within each redshift bin. The thin lines are the 10%, 25%, 50%, 75%, and 90% quantiles of the distribution. The thick line is the prediction of the model. The u band is not included in the fit, and the u magnitudes of most LRGs are poorly known. The other colors fit the models reasonably well. This model, remember, is given incredible freedom, meaning that the above agreement is the best one can do with the stellar population synthesis code of Bruzual & Charlot (2003). [See the electronic edition of the Journal for a color version of this figure.]

one of the local minima but is not guaranteed to find the global minimum. Thus, the reader who tries to reproduce our results using our methods or others may (depending on their initial conditions) find different local minima of χ^2 than we do.

Once we have fit for b_{ij} using the training set, we can minimize equation (11) for any other galaxy using any nonnegative least-squares algorithm to determine a_{ki} (since the minimization of eq. [11] has a linear form in that case). When we do so here we use the beautifully simple iterative method of Sha et al. (2002).

3. RESULTS

3.1. An Example: The Luminous Red Galaxy Templates

We begin with the simplest case, which is fitting a single template to just the SDSS photometric data of the LRG sample (Eisenstein et al. 2001). For many of these galaxies, which extend to $r < 19.5$ and are intrinsically red, the u -band flux is extremely poorly measured, so we ignore the u band for all LRGs and only fit to g , r , i , and z fluxes using the SDSS “model” fluxes as described in Stoughton et al. (2002) and elsewhere. In this case we fit for the a_{i0} and b_{0j} coefficients in equation (11); we want just a single template, expressed by the b_{0j} coefficients, and a single scaling of its flux for each galaxy, expressed by a_{i0} .

Figure 1 shows the spectrum of the best-fit LRG. This template is constrained by data between about 3000 and 10000 Å. Outside that range it is an extrapolation; that is, it is simply the best-fit model prediction, but there are no data to verify the model there.

Figure 2 shows the star formation history corresponding to this best-fit LRG spectrum. The top panel shows the star formation per unit time as a function of look-back time. The bottom panel shows the mean metallicity of the forming stars as a function of time. When considering these plots and those below, remember that although these results are our best fit, the parameters are highly degenerate (especially in, e.g., neighboring age bins). We show these merely to illustrate the general nature of the fits.

Figure 3 shows the LRG colors as a function of redshift, with the best-fit template color overplotted as the smooth thick line. In the code described in § 7 we use the routine `sdss_kcorrect` (with the optional flag `/lrg`) to perform these fits. The best fit is a good fit to the data.

Note that in this example we have fitted a nonevolving template, which is inappropriate over this range of redshifts—even if it is a good fit to the colors! In principle, we can adjust the methods used here for the case of evolving templates, but we do not do so here.

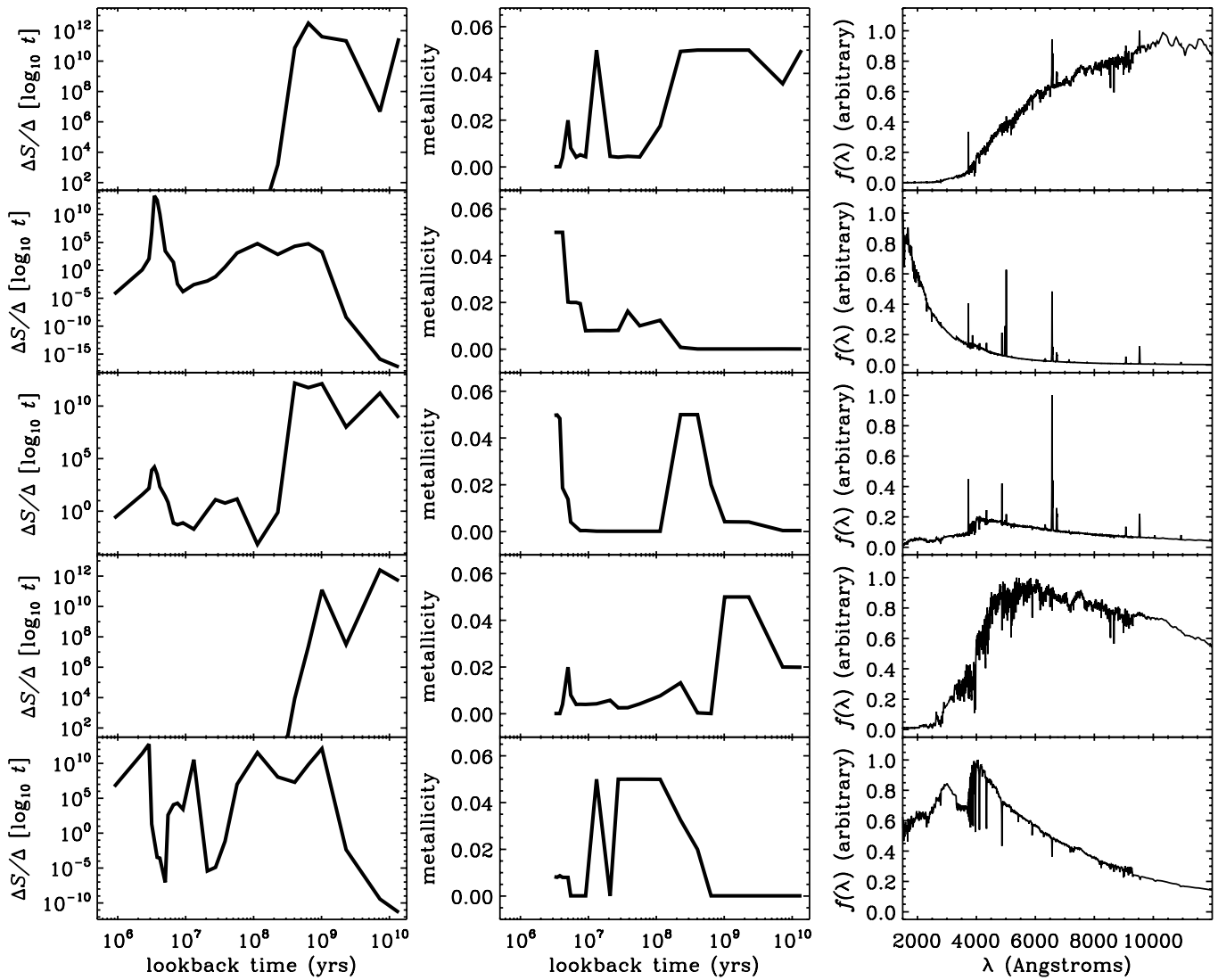


FIG. 4.—Similar to Fig. 2, but for the five global templates. Again, there are many degeneracies in the fit parameters (although there are fewer in the actual spectra), so these figures need to be interpreted appropriately.

In Appendix B we describe the form in which we release the star formation histories and spectra associated with this template.

3.2. Templates for the Full Data Set

We next apply the method to the full data set (i.e., all five items listed in § 2.3) and fit for five templates. From experiments, we found that we needed five to adequately explain the data. More than five templates would allow us to explain the data better, but only marginally so. Figure 4 (right panels) shows the spectrum from the ultraviolet through the NIR for the resulting templates. Note that there is a very old template, a very young template, and several intermediate templates, including one that is close to that of an A star.

Figure 4 (left and middle panels) shows the star formation histories and metallicities associated with the templates. We have not imposed any smoothness criterion on these histories, which explains the ragged appearance of these histories. The details of these fits are weakly constrained due to degeneracies within and among the templates, but we show them here for completeness.

In all the results below, we use these five templates unaltered. That is, when we speak below of fitting the templates, we mean we fix b_{ij} to the five templates shown in this section and fit only for a_{ki} . Since we have determined these templates to be appropriate

for the data sets we include in the training set, they end up providing good fits to most other galaxies from the parent data sets. In general below, the tests we perform are not to the training set but to independent sets of galaxies.

In Appendix B we describe the form in which we release the star formation histories and spectra associated with these templates.

3.3. Explanatory Power of Templates

These templates explain the photometric data rather well. For example, consider Figure 5, showing the color residuals of the observations with respect to the best fits, when fitting to galaxies with GALEX, SDSS, and 2MASS data (using sets of data analogous to those described in § 2.3 but in detail a different set of galaxies). In this context we define the color residuals as (for example)

$$\Delta[u - g] = [u_{\text{obs}} - g_{\text{obs}}] - [u_{\text{model}} - g_{\text{model}}]. \quad (12)$$

In the code described in § 7, we used the routine `gst_kcorrect` to perform these fits. In Figure 5 the thick dashed lines show the estimated 1σ uncertainties in the colors from the photometric catalogs. Relative to the uncertainties, there are no significant biases or redshift trends in these fits. Note that the galaxies used

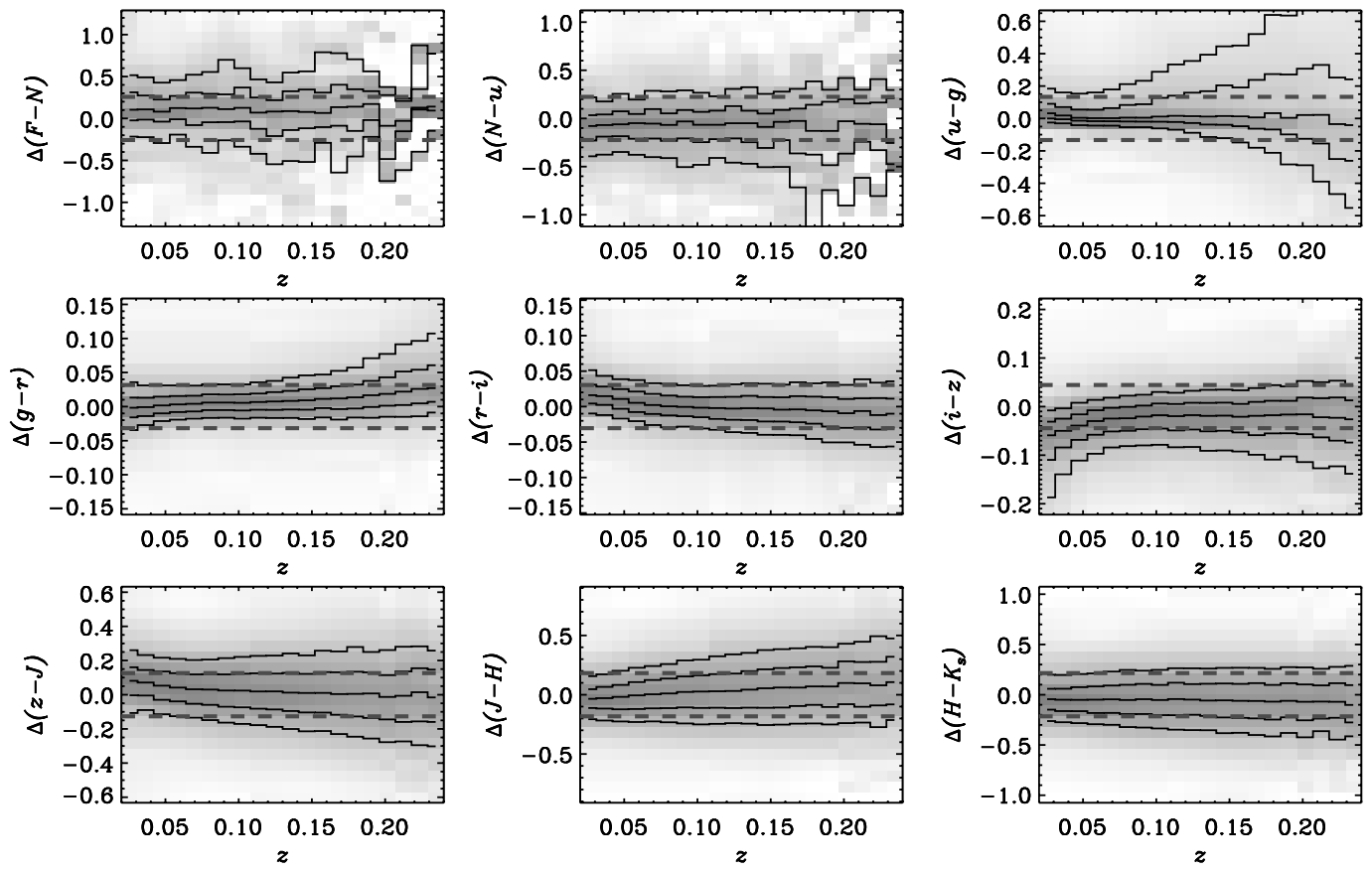


FIG. 5.—Color residuals (defined explicitly in the text) of *GALEX*, SDSS, and 2MASS observations relative to our best-fit five-template model. The gray scale is the conditional distribution of the color residual given the redshift. The thin lines are the 10%, 25%, 50%, 75%, and 90% quantiles of the distribution. The thick dashed lines show the estimated 1 σ uncertainties in the colors from the photometric catalogs. Relative to the uncertainties, there are no significant biases or redshift trends in these fits. [See the electronic edition of the *Journal for a color version of this figure.*]

in this test are distinct from the training set on which we fit the five templates.

The templates do well on higher redshift data as well. For example, Figure 6 shows the color residuals for GOODS data. Here we find that there are somewhat larger residuals with respect to the uncertainties (again shown as the thick dashed lines). We can compare this result to that in Figure 7, which we get by fitting a new set of templates to only the GOODS data (this alternate set of five templates is also distributed in the manner that Appendix B describes). From Figure 7 we conclude that some of the errors are irreducible, and either a different set of templates is required for high-redshift galaxies or there are simply errors in the catalogs or the input filter curves. For example, in the z and V bands we find significant trends between redshifts $z = 0.5$ and 1.5 (echoed in Fig. 6). More significantly, in the H band there is at least a 10% offset in the magnitudes across all redshifts, which is almost certainly a catalog or filter curve error. One possibility for these problems in the red is that intermediate-age populations have flux in the NIR from TP-AGB that our model omits; for example, Maraston (2005) has shown that such stars can significantly change the NIR colors. We defer a fuller investigation of these discrepancies. Other errors (such as a large scatter in the residuals in the B band and some redshift dependence in the J band) are clearly due to the fact that the templates are not primarily designed for GOODS data. All in all, we recommend using the special templates for K -corrections within the GOODS data set.

We can also test how well these templates recover actual spectra given only photometry. To do so, we take eight random SDSS spectra (chosen to span color space), project them onto the $g, r,$

and i bandpasses, and then fit the five templates to just these three fluxes. Figure 8 compares the reconstructed model spectra to the original spectrum. The two agree well in general, although some features (like the emission lines) are not reproduced well. Naturally, this success is mostly due to the quality of the original stellar spectra used in the population-synthesis code of Bruzual & Charlot (2003). We are not suggesting that gri photometry contains as much information as the full spectra. However, these results do suggest that by using broadband data we can infer K -corrections of galaxies.

3.4. Predictive Power of Templates

Perhaps more interestingly, the templates do a good job of predicting missing data. That is, we can ask the question: If we use the templates to fit only to some bands but leave out others, how well do the best fits predict the bands left out?

Consider Figures 9 and 10. The former shows the color residuals of fitting to both SDSS and 2MASS data for each galaxy. The latter shows the color residuals when we fit only to the SDSS data and do not include 2MASS in the fit at all. Without any input from 2MASS the templates do a very good job of predicting the 2MASS fluxes, with a scatter of 20%–30%, not far from the uncertainties in the 2MASS fluxes themselves.

However, we note here that this result flies in the face of the view of many that NIR observations are necessary to measure stellar masses of galaxies. If we can predict the NIR observations themselves, clearly they cannot be adding much to our knowledge of the underlying stellar mass. This fact changes one's decisions about what data are best to use for calculating the stellar mass

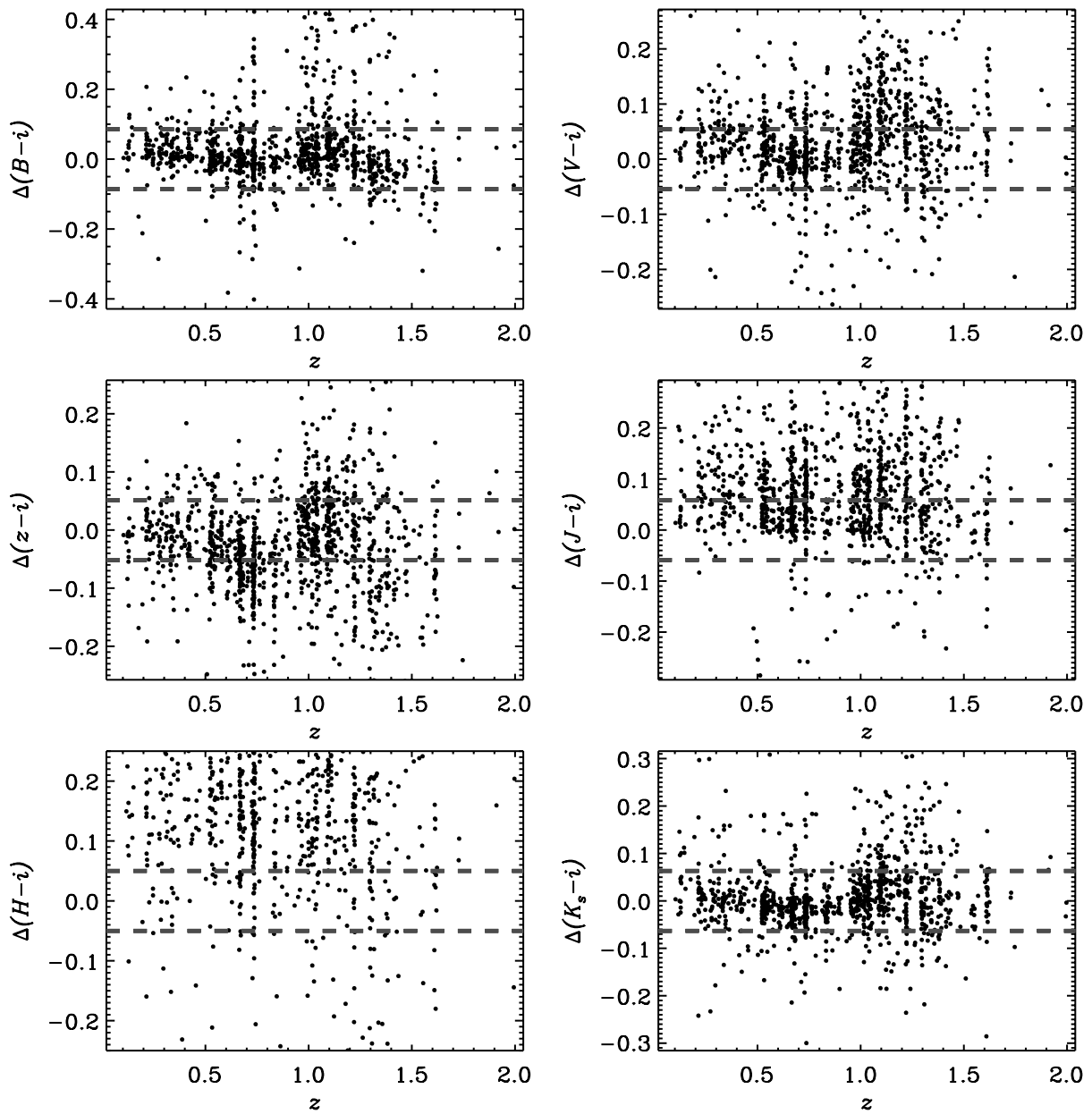


FIG. 6.—Color residuals in fit using the standard five templates to GOODS data, compared to the typical uncertainties (thick dashed lines). Note that the fits always do poorly on the H band, which we believe to be a catalog error. [See the electronic edition of the Journal for a color version of this figure.]

function. Basing it on 2MASS data only improves slightly the stellar mass estimate of each galaxy, while restricting (and thus biasing) the sample significantly at the lowest luminosities and surface brightnesses relative to the SDSS. Of course, if at high redshift galaxies have a very different locus of their SEDs (e.g., as perhaps is true of the GOODS galaxies in the NIR), then perhaps this statement is less true for them.

In addition, consider Figures 11 and 12. The former shows the color residuals of fitting to both SDSS and *GALEx* data for each galaxy. The latter shows the color residuals when we fit only to the SDSS data and do not include *GALEx* in the fit at all. Without any input from *GALEx* the templates do a significantly worse job at predicting the *GALEx* fluxes. The scatter becomes about $\sigma \sim 0.5$ mag. As is common knowledge, it is more difficult to predict the UV fluxes, because dust and recent star formation are so variable among galaxies. However, the median residuals our templates are based on are still near zero.

4. DETERMINING K-CORRECTIONS

Given a model spectrum for the galaxy, the determination of the K -correction is straightforward. Here we give the relevant formulae for the K -corrections, leaving the derivation to Hogg et al. (2002). Then, we show the typical K -corrections for the data to which we have fitted.

The K -correction between a bandpass R used to observe a galaxy at redshift z and the desired bandpass Q is defined by the equation (Oke & Sandage 1968; Hogg et al. 2002)

$$m_R = M_Q + \text{DM}(z) + K_{QR}(z) - 5 \log h, \quad (13)$$

where $\text{DM}(z) = 25 + 5 \log[d_L/(h^{-1} \text{ Mpc})]$ is the bolometric distance modulus calculated from the luminosity distance d_L , and M_Q is the absolute magnitude. The absolute magnitude is defined as the apparent magnitude an object would have if were observed

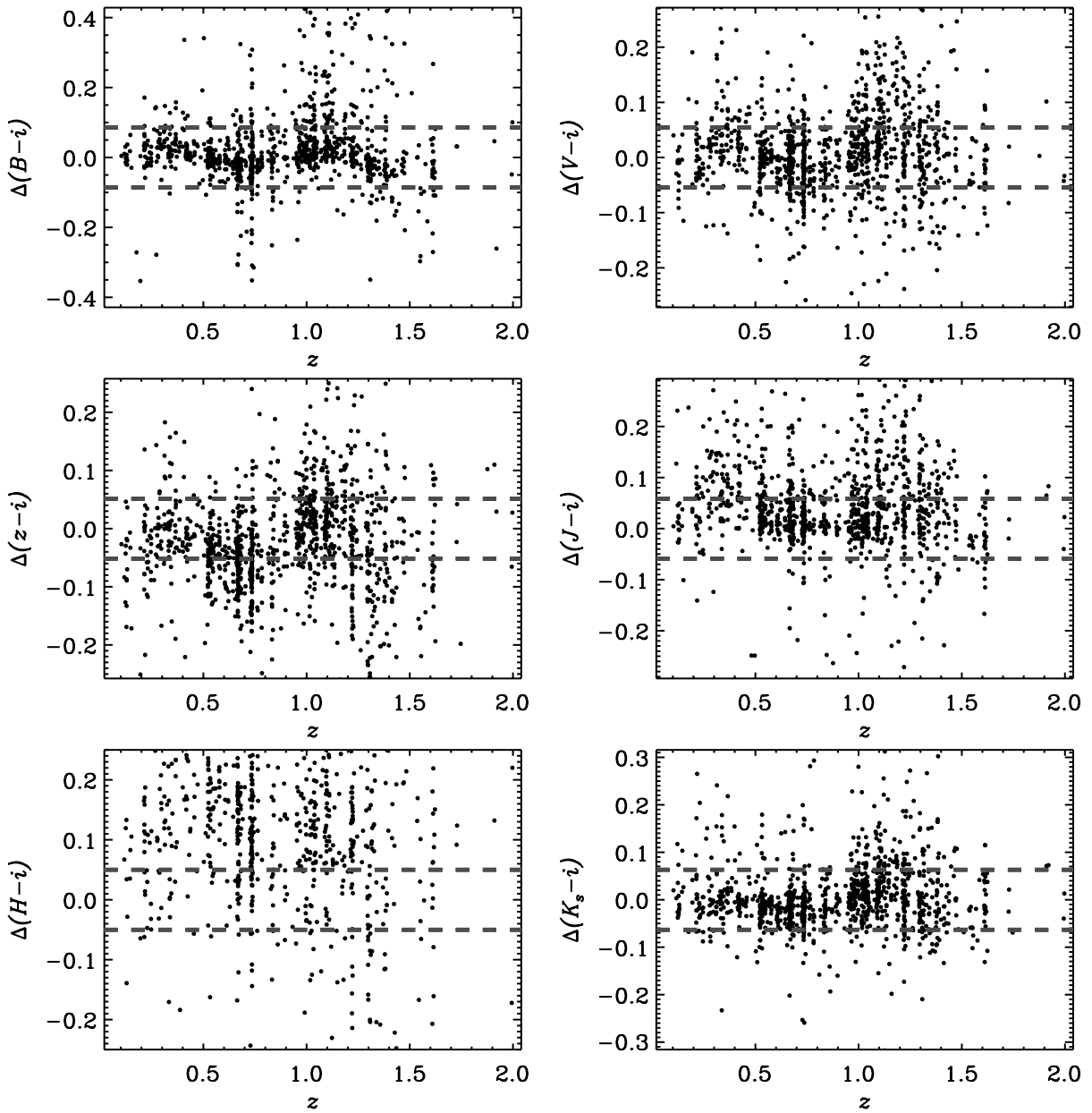


FIG. 7.—Same as Fig. 6, but fitting using five templates specially designed for GOODS. These templates have smaller residuals in many respects but still fail to fit the H -band data. [See the electronic edition of the Journal for a color version of this figure.]

10 pc away, in bandpass Q , at rest. The traditional definition of the K -correction takes $Q = R$. However, we note that in practice many surveys do perform K -corrections from one observed bandpass R to another bandpass Q in the rest frame. This practice is particularly common when dealing with high-redshift observations. In addition to K -corrections this method also provides an interpretation of the data in terms of a physical model that describes the stellar mass and star formation history of each galaxy.

Equation (13) holds if the K -correction K_{QR} is

$$K_{QR} = -2.5 \log \left[\frac{1}{(1+z)} \times \frac{\int d\lambda_o \lambda_o L_\lambda(\lambda_o/1+z) R(\lambda_o) \int d\lambda_e \lambda_e g_\lambda^R(\lambda_e) Q(\lambda_e)}{\int d\lambda_o \lambda_o g_\lambda^R(\lambda_o) R(\lambda_o) \int d\lambda_e \lambda_e L_\lambda(\lambda_e) Q(\lambda_e)} \right]. \quad (14)$$

Here $R(\lambda)$ and $Q(\lambda)$ represent the response of the instrument per unit photon entering Earth's atmosphere (or the telescope aperture for a space instrument), g_λ^R is the flux density per unit wavelength (e.g., ergs s⁻¹ cm⁻² Å⁻¹) for the standard source for band R , and g_λ^Q similarly for band Q . For example, if the magnitudes are AB relative, then these represent the AB standard source, while if they are Vega relative, then they represent the spectrum of Vega.

A particularly common special case is when $R = Q$:

$$K_R(z) = -2.5 \log \left[\frac{1}{(1+z)} \frac{\int d\lambda_o \lambda_o L_\lambda(\lambda_o/1+z) R(\lambda_o)}{\int d\lambda_e \lambda_e L_\lambda(\lambda_e) R(\lambda_e)} \right]. \quad (15)$$

For example, consider Figures 13, 14, and 15. For a randomly selected set of galaxies these figures show the K -corrections from the observed-frame bandpasses of *GALEX*, 2MASS, and SDSS respectively, to the same bandpasses in the rest frame.

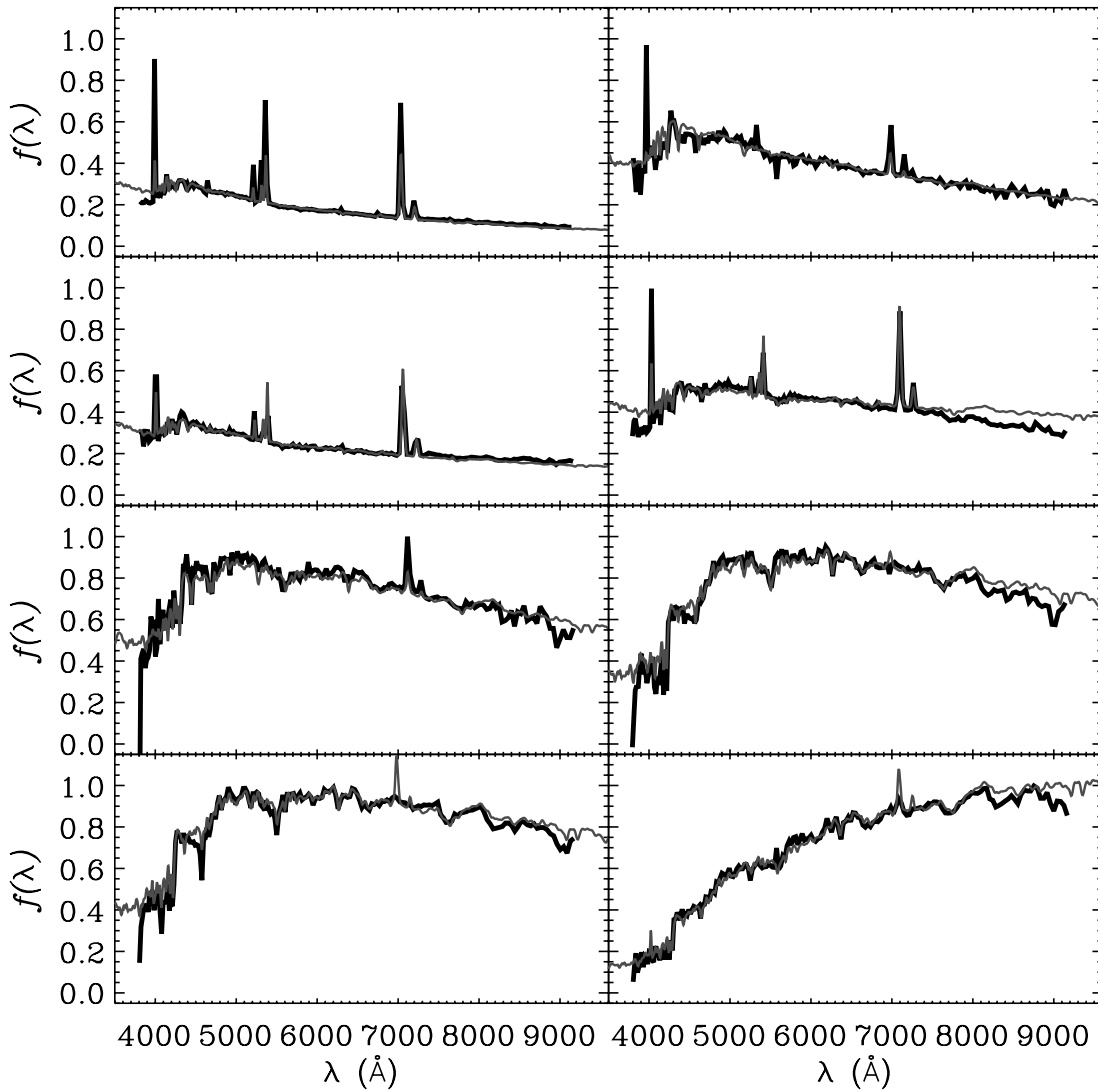


FIG. 8.—Best-fit model spectra based on the five-template fit to g , r , and i fluxes compared to the original SDSS spectra from which we computed those fluxes. The models and the original spectra agree very well. [See the electronic edition of the Journal for a color version of this figure.]

Often, it makes sense to K -correct to a different set of bandpasses than the rest frame. For example, the SDSS main sample is mostly around $z = 0.1$, so it does not always make sense to K -correct from the observed-frame r band to the rest-frame r band. Doing so means applying large and uncertain corrections to all galaxies. If precision is not important, this uncertainty might be worth the simplification it brings. However, if one is (for instance) interested in the evolution of galaxies, the clustering of galaxies, or something else that requires precision, it makes more sense to avoid introducing unnecessary uncertainty.

Our solution to this problem is to correct the magnitude to blueshifted bandpasses that correspond to the observed bandpass at some intermediate redshift. We denote these bandpasses ${}^z b$, where the blueshift in this case is by a factor $1 + z$. For example, in the case of SDSS galaxies it makes sense to correct to the ${}^{0.1}r$ bandpass, the r band blueshifted to $z = 0.1$. This bandpass has the property that the K -correction is independent of the SED of the galaxy. If the magnitudes are AB relative, then the K -correction to ${}^z b$ for a galaxy at redshift z is simply $-2.5 \log(1 + z)$.

Figure 16 shows the K -corrections from the $[ugriz]$ bands to the ${}^{0.1}[ugriz]$ bands as a function of redshift for SDSS galaxies. Note that the K -corrections converge at $z = 0.1$, so that around

that redshift (where most galaxies are) the uncertainties in the K -corrections are minimized. Compare this simplicity to Figure 15, in which the K -corrections at redshift $z = 0.1$ in the g band range between 0 and 0.2 (and in the u band from 0 to 0.5). Most SDSS galaxies are near redshift $z = 0.1$, and obviously the K -corrections are not perfect; why introduce a large uncertainty for most galaxies when it can easily be avoided?

5. PHYSICAL INTERPRETATION OF THE MODELS

In addition to K -corrections, these template fits also provide physical interpretations of the galaxies, since they correspond to actual stellar population synthesis models. Indeed, the code outputs three parameters relevant to the star formation history: the current mass of stars in the galaxy, the stellar mass-to-light ratio of the galaxy, and the fraction of the total amount of star formation that has occurred recently. We do not believe that fitting just to broadband colors can ever give extremely accurate values for these quantities, but to evaluate what `kcorrect` does in this regard we here examine the consistency between our results and those of other groups for the same galaxies.

Kauffmann et al. (2003) have also calculated stellar masses for SDSS galaxies. Roughly, they have calculated the z -band stellar

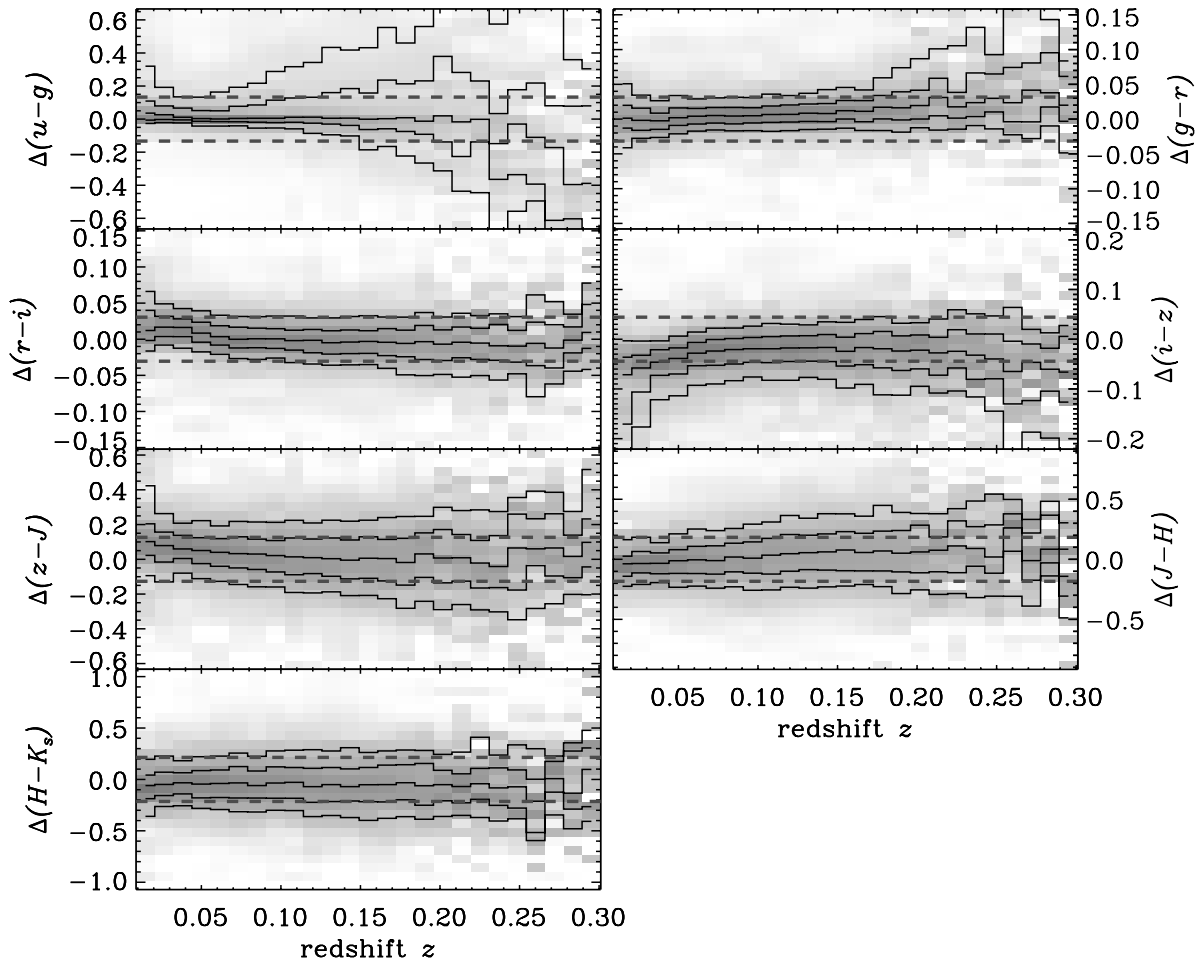


FIG. 9.—Similar to Fig. 5, but for galaxies observed in both SDSS and 2MASS and only using SDSS and 2MASS bands. The fits are to the SDSS and 2MASS data together. [See the electronic edition of the Journal for a color version of this figure.]

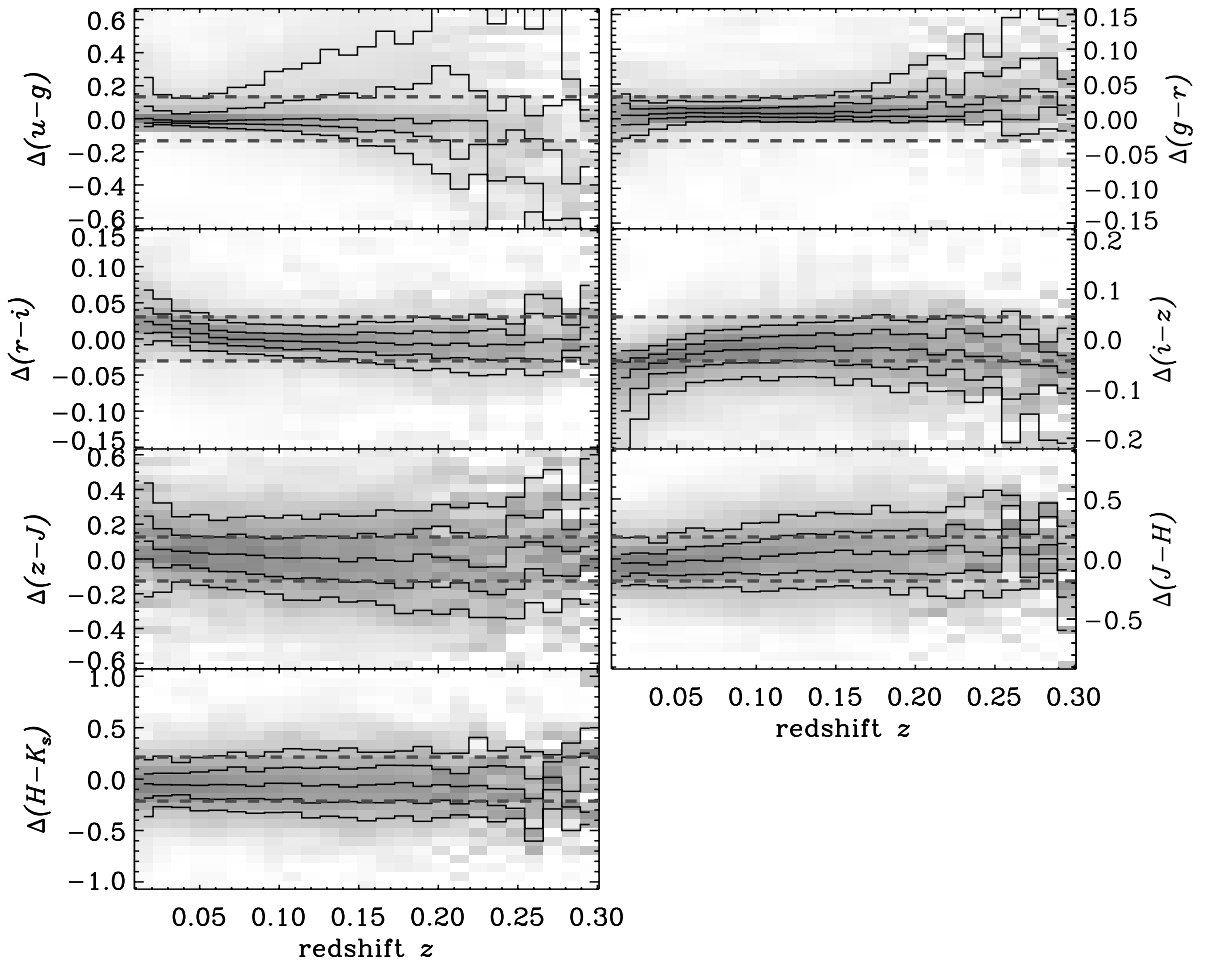


FIG. 10.—Similar to Fig. 9, but with fits only to the SDSS bands. The residuals in the 2MASS bands remain very small, indicating that the 2MASS measurements do not add a lot of information about these galaxies. [See the electronic edition of the Journal for a color version of this figure.]

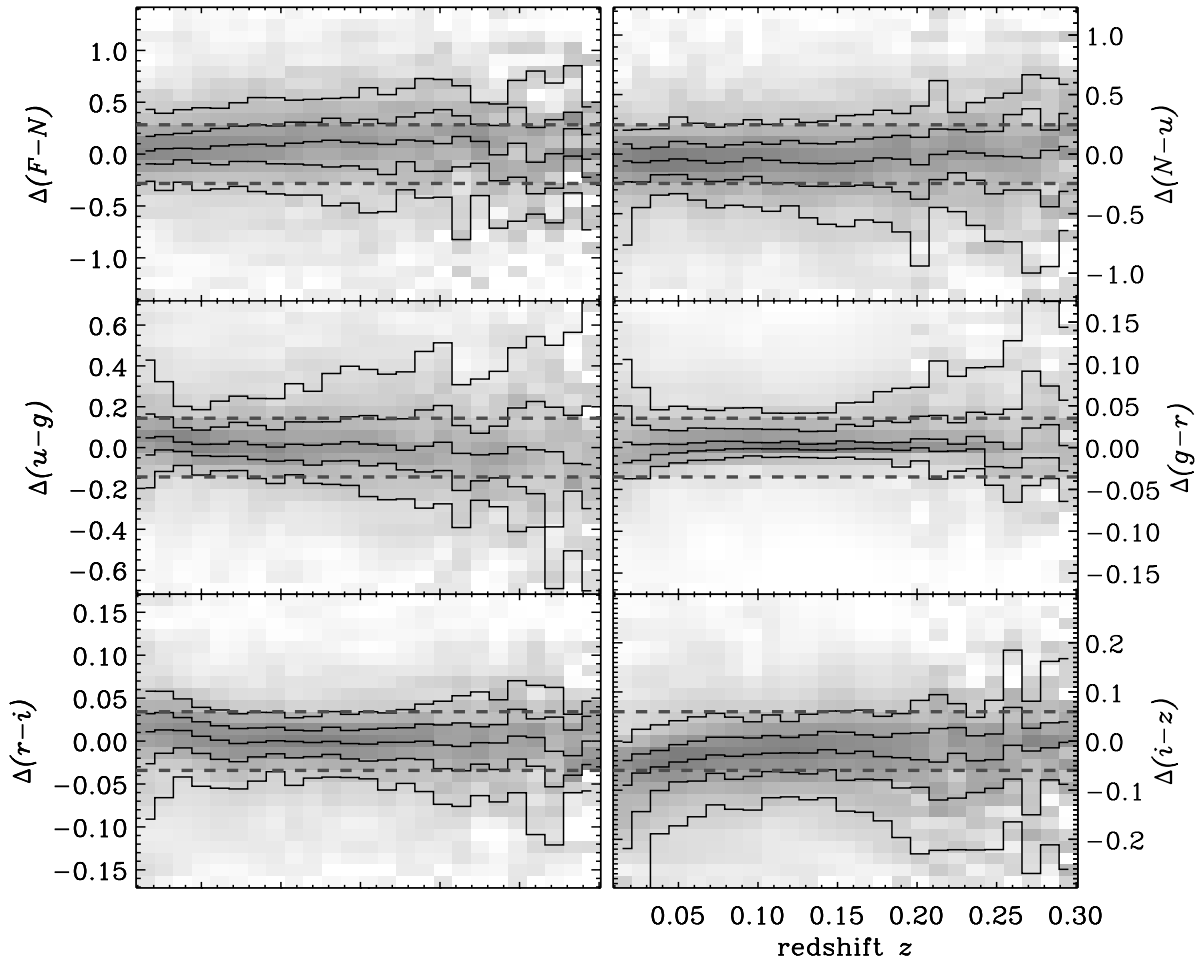


FIG. 11.—Similar to Fig. 9, but for galaxies observed in both SDSS and *GALEX* and only using SDSS and *GALEX* bands. The fits are to the SDSS and *GALEX* data together. [See the electronic edition of the Journal for a color version of this figure.]

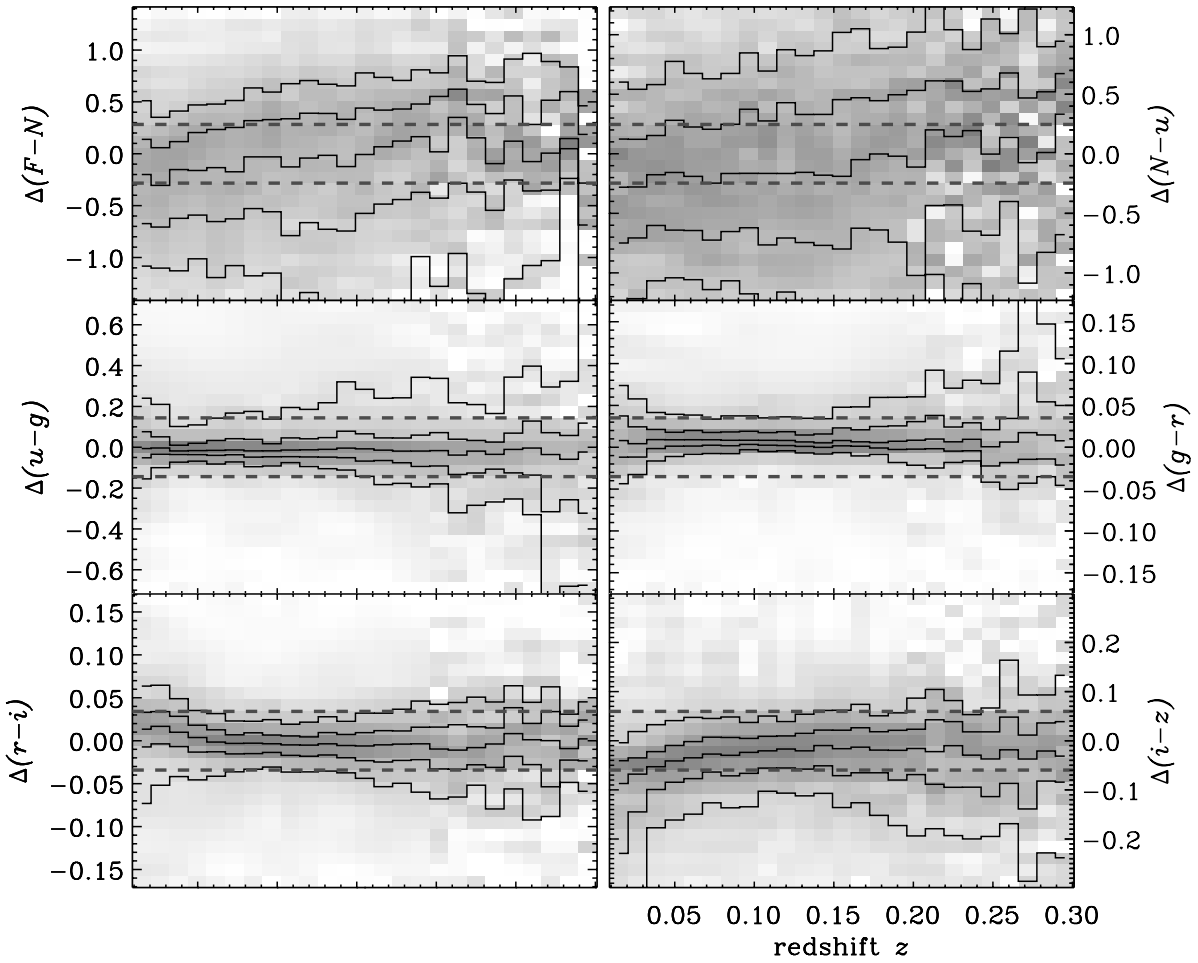


FIG. 12.—Similar to Fig. 11, but with fits only to the SDSS bands. [See the electronic edition of the Journal for a color version of this figure.]

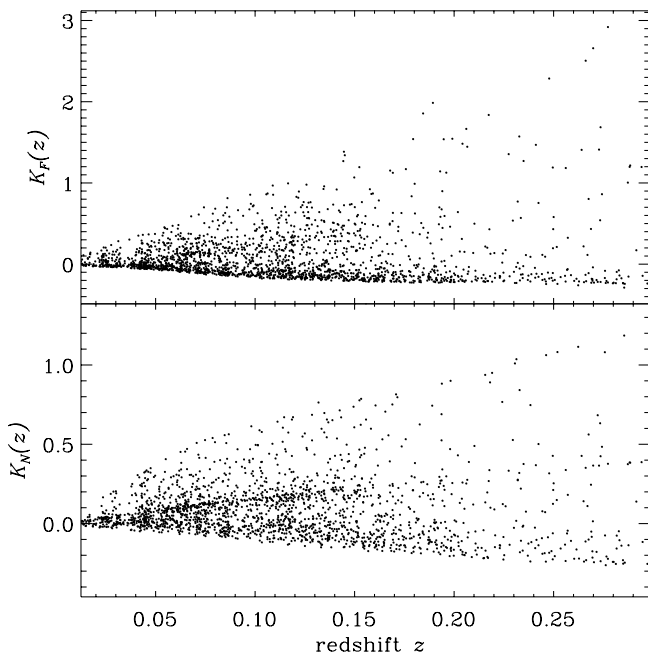


FIG. 13.— K -corrections as a function of redshift in the *GALEX* near- and far-UV bands.

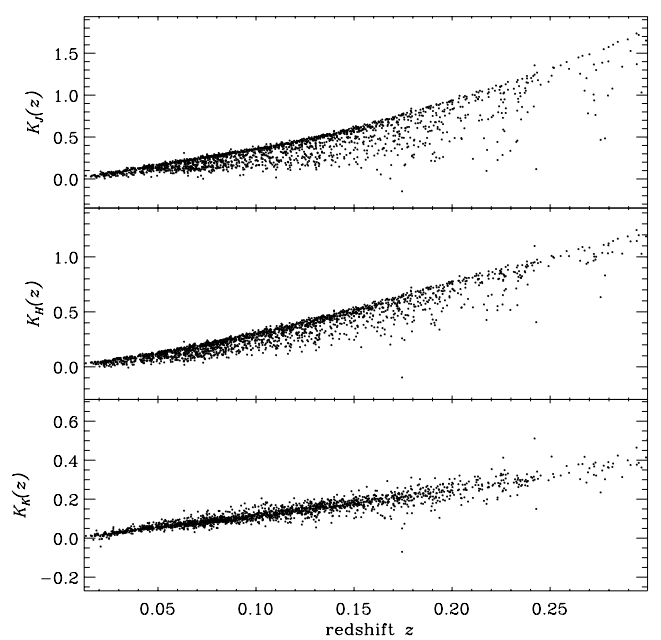


FIG. 14.— K -corrections as a function of redshift in the 2MASS J , H , and K_s bands.

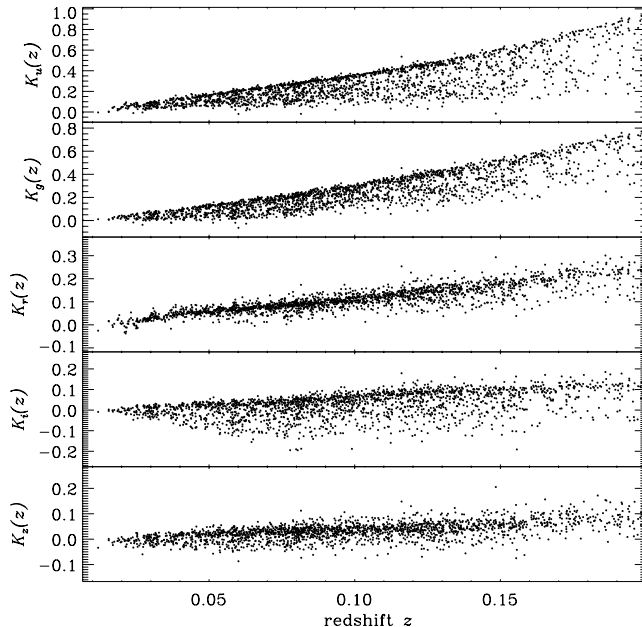


FIG. 15.— K -corrections as a function of redshift in the SDSS u , g , r , i , and z bands.

mass-to-light ratios of models that best fit the H δ absorption and D4000 measurements of the spectra and then applied those mass-to-light ratios to the observed z -band luminosities of the imaging. Figure 17 shows a galaxy-by-galaxy comparison of their stellar masses $M_{*,s}$ relative to our M_* as a function of M_* and of intrinsic $g - r$ color. The two sets of masses are very similar to each other, with a scatter of only 0.1 dex and trends of less than 0.2 dex with stellar mass. To be explicit, the masses in Figure 17 correspond to the current mass in stars remaining in the galaxy. This mass can differ from the total star formation rate integrated over time, due to the fact that stars can die, and in practice for our fits the total integrated star formation rate is usually about twice as high as the total current mass in stars.

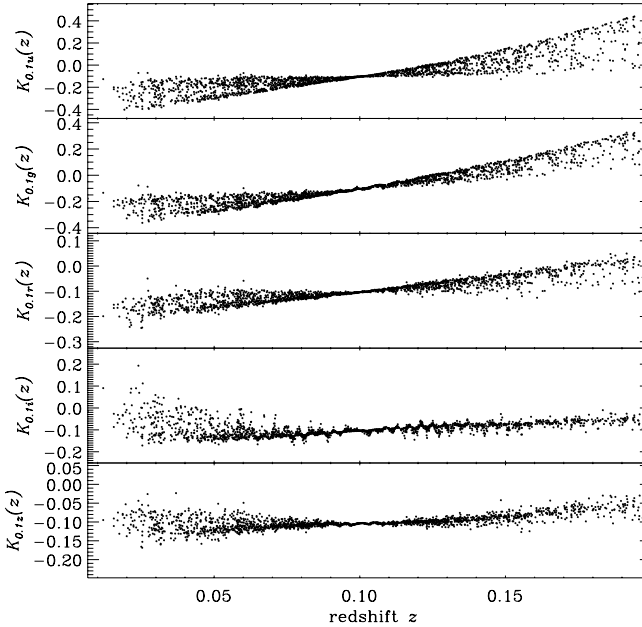


FIG. 16.—Same as Fig. 15, but K -correcting to the $0.1u$, $0.1g$, $0.1r$, $0.1i$, and $0.1z$ bands.

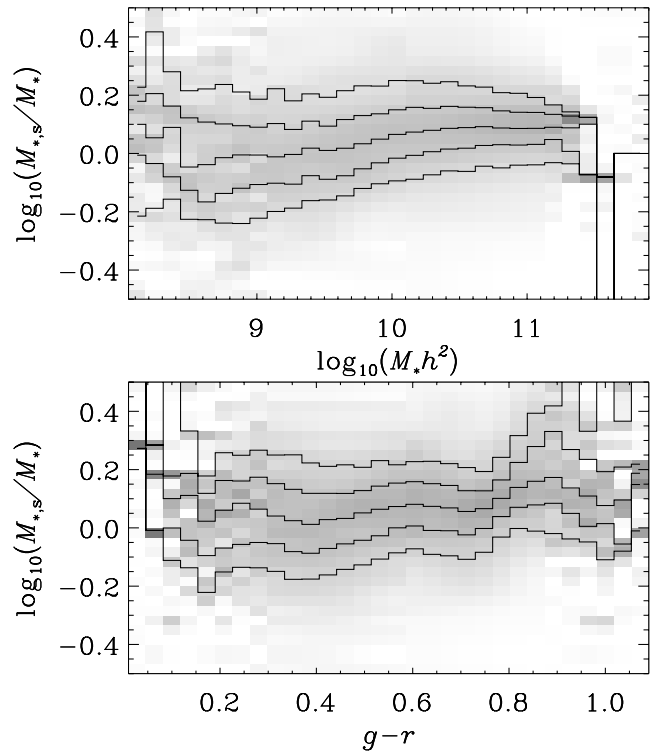


FIG. 17.—Our galaxy stellar mass estimates, M_* , compared to those of Kauffmann et al. (2003), $M_{s,*}$, as a function of stellar mass (top) and of color (bottom). The gray scale is the conditional distribution $M_{s,*}/M_*$ on each quantity. The lines are the 10%, 25%, 50%, 75%, and 90% quantiles.

Similarly, Figure 18 shows the mass-to-light ratios of SDSS galaxies in the V band as a function of color in $B - V$. Here, we have calculated the B - and V -band fluxes based on the template fits to each galaxy, as explained in § 6 below. We give the mass-to-light ratio in solar units. The solid line is the relationship that

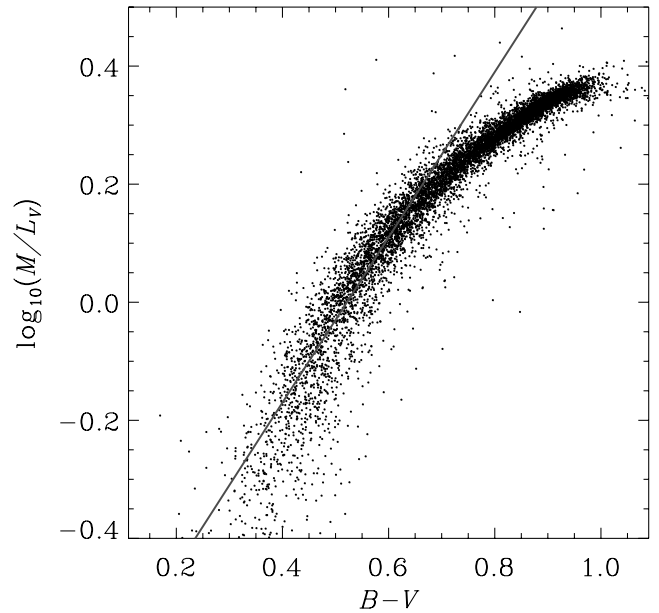


FIG. 18.—Mass-to-light ratios of galaxies in the V band (in solar units) as a function of galaxy $B - V$ color. The solid line satisfies the relationship $\log(M/L_V) = 1.40(g - r) - 0.73$, given by Bell & de Jong (2001) for their sample of spiral galaxies. Their estimates and ours agree for $B - V < 0.8$, where spiral galaxies dominate the galaxy population. [See the electronic edition of the Journal for a color version of this figure.]

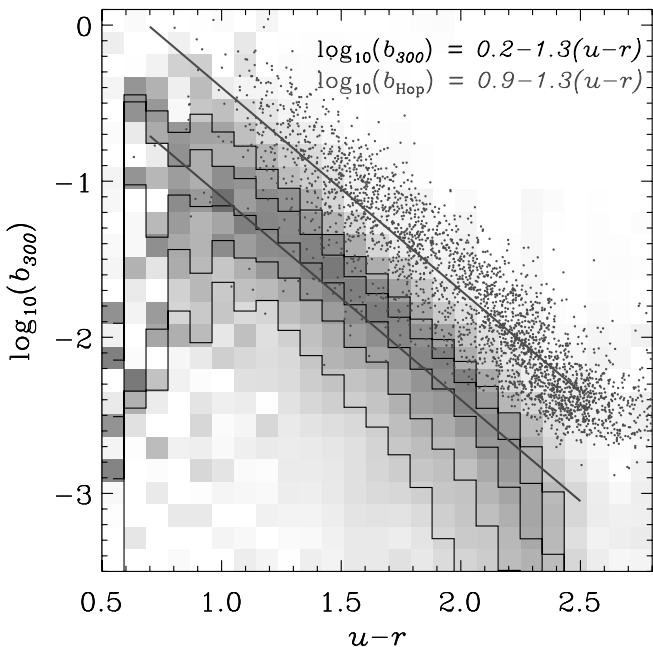


FIG. 19.—Fraction of the total star formation that has occurred in the previous 300 Myr, b_{300} , as a function of rest-frame $u - r$ color, for SDSS galaxies. The gray scale is the conditional distribution of b_{300} on $u - r$. The lines are the 10%, 25%, 50%, 75%, and 90% quantiles. For comparison we show the results of using the scaling of Hopkins et al. (2003). [See the electronic edition of the Journal for a color version of this figure.]

Bell & de Jong (2001) gave based on their fits to spiral galaxies. For blue galaxies ($B - V < 0.8$) this line is indeed a good fit to our results. For the typical red galaxy, the Bell & de Jong (2001) relation predicts a larger stellar mass than we do.

Finally, we can also calculate measures of the recent star formation rate from these fits. Since our fits are to broadband photometry, and not based on emission-line measurements, we cannot expect to have detailed information about the very recent star formation rate. However, we can try to measure what fraction of the total star formation has occurred in, e.g., the past 300 Myr:

$$b_{300} = \frac{\int_0^{300 \text{ Myr}} dt \text{SFR}(t)}{\int_0^{a_{\text{univ}}} dt \text{SFR}(t)}, \quad (16)$$

where the definition here is meant to be similar to the birthrate parameter b in Kennicutt et al. (1994 and references therein). Note that here b_{300} is defined in terms of the total integrated star formation history (unlike the stellar masses referred to above) as is standard for the b parameter. Figure 19 shows the relationship between the rest-frame $u - r$ color for SDSS galaxies and b_{300} . For our results, the median relationship is close to

$$\log b_{300} = 0.2 - 1.3(u - r). \quad (17)$$

Note, however, the large scatter (about 0.3 dex at 1σ). The overlaid points show the results of using the formula of Hopkins et al. (2003) to infer the current star formation rate from the u band, integrating over 300 Myr, scaling by the integrated stellar mass from the kcorrect determination, and then correcting for the internal u -band dust extinction inferred by the kcorrect fits (which turns out to be factors ranging from 3 to 10, similar to the factors used by Hopkins et al. [2003]). Our results roughly scale as those of Hopkins et al. (2003) do, but with lower star formation rates by a factor of 5 or so. Since Hopkins et al. (2003) calibrated their star

TABLE 1
PROPERTIES OF VARIOUS FILTERS

Band	λ_{eff} (Å)	$m_{\text{AB}} - m_{\text{Vega}}$	M_{\odot} (AB)	M_{\odot} (Vega)
U	3571	0.79	6.35	5.55
B	4344	-0.09	5.36	5.45
V	5456	0.02	4.80	4.78
R	6442	0.21	4.61	4.41
I	7994	0.45	4.52	4.07
u	3546	0.91	6.38	5.47
g	4670	-0.08	5.12	5.20
r	6156	0.16	4.64	4.49
i	7472	0.37	4.53	4.16
z	8917	0.54	4.51	3.97
J	12355	0.91	4.56	3.65
H	16458	1.39	4.71	3.32
K_s	21603	1.85	5.14	3.29
$0.1u$	3224	1.25	6.78	5.53
$0.1g$	4245	-0.01	5.43	5.44
$0.1r$	5597	0.04	4.76	4.71
$0.1i$	6792	0.27	4.57	4.30
$0.1z$	8107	0.46	4.52	4.05

NOTES.—Table 1 uses the model solar spectrum and model Vega spectrum of Kurucz (1991). Effective wavelength is defined in the text. The $UBRVI$ filters are those of Bessell (1990). The $ugriz$ filters are those determined by M. Doi, D. Eisenstein, and J. Gunn and are available on the SDSS DR4 Web site (<http://www.sdss.org/dr4/>). The JHK_s filters are those from Cohen et al. (2003).

formation rates to a number of other indicators, we conclude that kcorrect probably underestimates the recent star formation rate.

We do not want to overstate the validity of these physical interpretations. They are sufficiently good physical interpretations to explain broadband data, but not uniquely so. Certainly more detailed spectroscopic analysis can provide better constraints on star formation histories and stellar masses. However, the results from kcorrect are roughly in agreement with what other authors find with comparable data.

One particular weakness for high-redshift data is that the templates always assume that there are 14 Gyr of star formation history. Thus, kcorrect may greatly overestimate the stellar masses of galaxies at $z \sim 1$ (for example), where the actual star formation history must last only 6 Gyr.

6. LINEAR RELATIONSHIPS BETWEEN COMMON MAGNITUDE SYSTEMS

The software and templates that we present here are also useful for determining simple conversions between bandpasses performing other common tasks, such as calculating the absolute magnitude of the Sun in various band systems and calculating the conversion between Vega and AB magnitudes. In this section we present these tools.

For example, Table 1 lists the effective wavelengths, conversion from Vega to AB magnitudes, and absolute magnitudes of the Sun in a number of filters: the GALEX filters, the Bessell filters, the SDSS filters, and the 2MASS filters. The listed numbers are the results of running the IDL functions `k_lambda_eff`, `k_vega2ab`, and `k_solar_magnitudes`, respectively, so the reader can calculate the same thing easily on any given filter. The effective wavelengths listed for each filter use the definition

$$\lambda_{\text{eff}} = \exp \left[\frac{\int d(\ln \lambda) R(\lambda) \ln \lambda}{\int d(\ln \lambda) R(\lambda)} \right], \quad (18)$$

TABLE 2
CONVERSIONS AMONG VARIOUS FILTERS

Equation	Color Dispersion
$u = {}^{0.1}u - 0.3310 - 0.3014[({}^{0.1}u - {}^{0.1}g) - 1.2839]$	$\sigma[{}^{0.1}u - {}^{0.1}g] = 0.28$
$g = {}^{0.1}g - 0.3112 - 0.3530[({}^{0.1}g - {}^{0.1}r) - 0.7187]$	$\sigma[{}^{0.1}g - {}^{0.1}r] = 0.20$
$r = {}^{0.1}r - 0.2026 - 0.3810[({}^{0.1}r - {}^{0.1}i) - 0.3530]$	$\sigma[{}^{0.1}r - {}^{0.1}i] = 0.07$
$i = {}^{0.1}i - 0.1072 - 0.4273[({}^{0.1}i - {}^{0.1}z) - 0.1914]$	$\sigma[{}^{0.1}i - {}^{0.1}z] = 0.13$
$z = {}^{0.1}i - 0.3161 - 1.2057[({}^{0.1}i - {}^{0.1}z) - 0.1914]$	$\sigma[{}^{0.1}i - {}^{0.1}z] = 0.13$
$u = U + 0.0682 + 0.0197[(U - B) - 0.9602]$	$\sigma[U - B] = 0.20$
$g = B - 0.2354 - 0.3411[(B - V) - 0.5870]$	$\sigma[B - V] = 0.18$
$r = V - 0.2585 - 0.5003[(V - R) - 0.3161]$	$\sigma[V - R] = 0.07$
$i = R - 0.2000 - 0.4248[(R - I) - 0.2652]$	$\sigma[R - I] = 0.12$
$z = R - 0.4088 - 1.2495[(R - I) - 0.2652]$	$\sigma[R - I] = 0.12$
${}^{0.1}u = U + 0.3989 + 0.4135[(U - B) - 0.9602]$	$\sigma[U - B] = 0.20$
${}^{0.1}g = U - 0.8845 - 0.9508[(U - B) - 0.9602]$	$\sigma[U - B] = 0.20$
${}^{0.1}g = B + 0.0759 + 0.0620[(B - V) - 0.5870]$	$\sigma[B - V] = 0.18$
${}^{0.1}r = B - 0.6429 - 1.0845[(B - V) - 0.5870]$	$\sigma[B - V] = 0.18$
${}^{0.1}r = V - 0.0558 - 0.1803[(V - R) - 0.3161]$	$\sigma[V - R] = 0.07$
${}^{0.1}i = R - 0.0927 + 0.0035[(R - I) - 0.2652]$	$\sigma[R - I] = 0.12$
${}^{0.1}z = R - 0.2841 - 1.0301[(R - I) - 0.2652]$	$\sigma[R - I] = 0.12$
${}^{0.1}u = u + 0.3310 + 0.3203[(u - g) - 1.2638]$	$\sigma[u - g] = 0.26$
${}^{0.1}g = u - 0.9528 - 0.7572[(u - g) - 1.2638]$	$\sigma[u - g] = 0.26$
${}^{0.1}g = g + 0.3113 + 0.4620[(g - r) - 0.6102]$	$\sigma[g - r] = 0.15$
${}^{0.1}r = g - 0.4075 - 0.8577[(g - r) - 0.6102]$	$\sigma[g - r] = 0.15$
${}^{0.1}i = r - 0.1504 - 0.3654[(r - i) - 0.2589]$	$\sigma[r - i] = 0.10$
${}^{0.1}z = i - 0.0836 - 0.7518[(i - z) - 0.2083]$	$\sigma[i - z] = 0.10$
$U = u - 0.0682 - 0.0140[(u - g) - 1.2638]$	$\sigma[u - g] = 0.26$
$B = u - 1.0286 - 0.7981[(u - g) - 1.2638]$	$\sigma[u - g] = 0.26$
$B = g + 0.2354 + 0.3915[(g - r) - 0.6102]$	$\sigma[g - r] = 0.15$
$V = g - 0.3516 - 0.7585[(g - r) - 0.6102]$	$\sigma[g - r] = 0.15$
$R = r - 0.0576 - 0.3718[(r - i) - 0.2589]$	$\sigma[r - i] = 0.10$
$I = i - 0.0647 - 0.7177[(i - z) - 0.2083]$	$\sigma[i - z] = 0.10$
$U = {}^{0.1}u - 0.3992 - 0.3189[({}^{0.1}u - {}^{0.1}g) - 1.2839]$	$\sigma[{}^{0.1}u - {}^{0.1}g] = 0.28$
$B = {}^{0.1}g - 0.0759 - 0.0545[({}^{0.1}g - {}^{0.1}r) - 0.7187]$	$\sigma[{}^{0.1}g - {}^{0.1}r] = 0.20$
$V = {}^{0.1}g - 0.6628 - 0.9259[({}^{0.1}g - {}^{0.1}r) - 0.7187]$	$\sigma[{}^{0.1}g - {}^{0.1}r] = 0.20$
$R = {}^{0.1}r - 0.2603 - 0.9162[({}^{0.1}r - {}^{0.1}i) - 0.3530]$	$\sigma[{}^{0.1}r - {}^{0.1}i] = 0.07$
$I = {}^{0.1}i - 0.1725 - 0.9718[({}^{0.1}i - {}^{0.1}z) - 0.1914]$	$\sigma[{}^{0.1}i - {}^{0.1}z] = 0.13$

NOTE.—Table 2 uses AB magnitudes throughout.

following Fukugita et al. (1996) and Schneider et al. (1983). For the spectrum of Vega in the conversion of AB to Vega magnitudes, we use the Kurucz (1991) theoretical Vega spectrum (normalized at 5000 Å to match the Hayes [1985] spectrophotometry of Vega). In `k_vega2ab` the user has the option to use the spectrum of Hayes (1985) instead. We use the solar spectrum of Kurucz (1991) for the calculation of the solar absolute magnitude.

For comparison among results from different surveys, one also wants to be able to convert the magnitudes in one set of bandpasses to magnitudes in another set of bandpasses. An example of doing so is given in our piece of code `sdss2besse11`, which takes SDSS input magnitudes and outputs absolute magnitudes in the Bessel U, B, V, R , and I bandpasses.

However, often one wants to just make quick and dirty comparisons, without going through the trouble of running any software. For these purposes, we provide Table 2, which provides the linear relationships among the same bandpasses as those listed in Table 1. In fact, these relationships are usually good to 0.05 mag or better. Note that Table 2 refers to AB magnitudes throughout; use Table 1 to get the relationships to Vega magnitudes.

7. SUMMARY

We have here described a method for fitting templates to nearly arbitrary sets of spectra and broadband fluxes. The basic concept is that we can recover a small set of templates (based on models),

nonnegative linear combinations of which can explain a much larger set of inhomogeneous observations. We have applied this method to SDSS, GALEX, 2MASS, DEEP2, and GOODS data to come up with a set of templates that are effective for describing all of these data sets.

Nonnegative matrix factorization (NMF) is an effective way to reduce the dimensionality of any large data set, and has that in common with PCA. It is, in some sense, a “nonnegative PCA.” However, at least in the current context the method has several advantages over PCA. First, it has a natural physical interpretation associated with that spectral subspace, which is the corresponding subspace of all possible star-formation histories. Second, it naturally handles data uncertainties and missing data, which allows it to ignore variation that is due purely to statistical errors. Third, it handles the complications of observing galaxy spectra photometrically using broadband filters.

We note here that the general NMF method does not depend on using a model; our “model” could just have been a set of top-hat functions or Gaussian functions on a wavelength grid. In some situations, such as data sets for which there are not well-developed theoretical models, this approach could be more appropriate.

We have released our results in the form of templates and a code base called `kcorrect`, which fits those templates to many types of data (SDSS photometric and spectroscopic data, GALEX data, GOODS data, DEEP2 data, and 2MASS data). Furthermore, this code returns K -corrections and a physical interpretation of the

photometry. All of the plots in this paper were created using code in the repository. The code is available from a Web page maintained by one of the authors.⁶ This Web page is kept updated on improvements in the code and new developments. It consists of a C language library, stand-alone C programs, and IDL language wrappers around the C library. Thus, one can use the basic templates and fitting code using only a machine with a C compiler. However, there is significant functionality that is programmed in the (unfortunately proprietary) IDL language. These routines depend on the `idlutils` library.⁷

The authors would like to thank Alison Coil, Michael Cooper, David W. Hogg, John Moustakas, Leonidas Moustakas, David Schiminovich, Risa Wechsler, Andrew West, and the anonymous referee for their detailed comments and feedback. This work was funded by a *GALEX* Archival Program (38) and an *HST* Archival Research grant (AR-9912). This publication makes use of data products from the Two Micron All Sky Survey, which is a joint project of the University of Massachusetts and the Infrared Processing and Analysis Center, California Institute of Technology, funded by the National Aeronautics and Space Administration and the National Science Foundation. The *Galaxy Evolution Explorer* is a NASA Small Explorer. The mission was developed in cooperation with the Centre National d'Etudes Spatiales of France and the Korean Ministry of Science and Technology. DEEP2 is a collaboration between University of California, Santa Cruz and University of California, Berkeley. Funding for the DEEP2 survey has been provided by NSF grants AST 00-71048 and AST 00-71198. Funding for the creation and distribution of the SDSS Archive has been provided by the Alfred P. Sloan Foundation, the Participating Institutions, the National Aeronautics and Space Administration, the National Science Foundation, the US Department of Energy, the Japanese Monbukagakusho, and the Max Planck Society. The SDSS Web site is <http://www.sdss.org>. The SDSS is managed by the Astrophysical Research Consortium for the Participating Institutions. The Participating Institutions are the University of Chicago, Fermilab, the Institute for Advanced Study, the Japan Participation Group, the Johns Hopkins University, Los Alamos National Laboratory, the Max Planck Institute for Astronomy, the Max Planck Institute for Astrophysics, New Mexico State University, Princeton University, the US Naval Observatory, and the University of Washington.

APPENDIX A

NONNEGATIVE MATRIX FACTORIZATION

A1. STANDARD NMF

The standard nonnegative matrix factorization (NMF) problem, as originally posed by Lee & Seung (2000), is to approximate a data matrix X (of size $N_k \times N_n$) as the outer product of two rank N_i nonnegative matrices W and H . For example, in this paper X represents the fluxes at N_n different wavelengths for N_k different galaxies, H represents a set of N_i templates to build each galaxy from, and W represents, for each galaxy, the weights to give each template. This factorization is similar in spirit to singular-value decomposition (SVD) and PCA, but crucially, in NMF, X , W , and H are all constrained to have nonnegative entries. This changes the problem fundamentally, since no “cancellation” of

positive and negative basis functions or coefficients is possible; all approximation interactions are strictly additive. The goal, as with SVD or PCA, is to minimize the squared approximation error (Frobenius norm):

$$\begin{aligned}\chi^2 &= \| X - WH \| ^2 \\ &= \sum_{kn} \left(X_{kn} - \sum_i W_{ki} H_{in} \right)^2.\end{aligned}\quad (\text{A1})$$

In their seminal papers, Lee & Seung (2000) showed that this approximation error is nonincreasing under the following very simple multiplicative update rules:

$$W_{ki} \leftarrow W_{ki} \frac{[XH^T]_{ki}}{[WHH^T]_{ki}}, \quad (\text{A2})$$

$$H_{in} \leftarrow H_{in} \frac{[W^T X]_{in}}{[W^T W H]_{in}}, \quad (\text{A3})$$

where $[M]_{ab}$ denotes the (ab) element of the matrix-valued expression M , and H^T is the transpose of matrix H .

These rules are remarkable because, although they make finite (not infinitesimal) adjustments to the elements of the approximation matrices, they have no step-size parameters and are always guaranteed to reduce the error (or leave it invariant once they have converged); χ^2 is in general a “nonconvex” function of W and H , meaning we cannot guarantee there is only one local minimum. Therefore, the procedure does not necessarily find the global optimum. But in practice, even with random initialization, these rules seem to converge to good solutions for real data (at least data like ours).

A2. NMF IN THE SPACE OF COEFFICIENTS FOR A KNOWN BASIS

The factorization problem we face in this paper is a slight variation on the basic NMF setup described above. We wish to approximate X by the product ABM , where M is a given (fixed) basis matrix of size $N_j \times N_n$ and the optimization is over the matrices A (of size $N_k \times N_i$) and B (of size $N_i \times N_j$). All matrices X , A , B , and M have nonnegative entries. This can be thought of as performing NMF on the coefficients of an approximation, given a fixed (non-negative) basis, described by the columns of M . Once again, the objective we wish to minimize is the squared approximation error:

$$\begin{aligned}\chi^2 &= \| X - ABM \| ^2 \\ &= \sum_{kn} \left(X_{kn} - \sum_{ij} A_{ki} B_{ij} M_{jn} \right)^2.\end{aligned}\quad (\text{A4})$$

This equation is almost that posed in equation (11). In the case of this paper, this generalization allows us to express the templates in terms of star formation histories, while comparing the predicted fluxes for the star formation histories through the M -matrix to the observed fluxes X .

Of course, in the very special case for which M is an invertible matrix, this problem can be transformed into the original NMF problem above by right multiplying the data matrix by M^{-1} . However, in most situations, including ours, M has many fewer rows than columns, and as such is far from invertible. Fortunately, however, it is possible to derive multiplicative updates for this extended problem that minimize the error directly, even when M is not invertible.

⁶ See <http://cosmo.nyu.edu/blanton/kcorrect>.

⁷ Available at <http://skymaps.info>.

First, by thinking of the tensor product BM as a single non-negative matrix H , we can trivially derive a multiplicative update equation for the elements of A by using the W update provided above:

$$A_{ki} \leftarrow A_{ki} \frac{[XM^T B^T]_{ki}}{[ABMM^T B^T]_{ki}}. \quad (\text{A5})$$

By Lee & Seung's (2000) original proof, this update is guaranteed (for any nonnegative matrices X , M , and B) not to increase the approximation error.

Our main algorithmic contribution is to derive a similar update equation for the elements of B ,

$$B_{ij} \leftarrow B_{ij} \frac{[A^T XM^T]_{ij}}{[A^T ABMM^T]_{ij}}. \quad (\text{A6})$$

Following the technique outlined in Lee & Seung (2000) it can still be shown that the error is nonincreasing under the application of this update.

The proof involves the use of an inequality lemma for symmetric nonnegative matrices:

LEMMA: *For any symmetric matrix P having nonnegative entries $P_{ni} \geq 0$, any vector z having nonnegative entries $z_n \geq 0$, and any vector y ,*

$$\sum_{ni} y_n z_i P_{ni} \leq \sum_{ni} y_n^2 \frac{z_i}{z_n} P_{ni}. \quad (\text{A7})$$

For the standard NMF problem, we can prove that the approximation error (eq. [A1]) is nonincreasing under equation (A2) by using the above lemma to construct a function $\phi(W, Z)$ that is an upper bound on the cost $\chi^2(W)$ for any nonnegative matrix Z :

$$\chi^2(W) = \sum_{knl} W_{ki} W_{kl} H_{in} H_{ln} - 2 \sum_{kni} W_{ki} X_{kn} H_{in} + \sum_{kn} X_{kn}^2, \quad (\text{A8})$$

$$\phi(W, Z) = \sum_{knl} W_{ki}^2 \frac{Z_{kl}}{Z_{ki}} H_{in} H_{ln} - 2 \sum_{kni} W_{ki} X_{kn} H_{in} + \sum_{kn} X_{kn}^2, \quad (\text{A9})$$

$$\phi(W, Z) \geq \chi^2(W) \quad \forall W_{ki} \geq 0, Z_{ki} \geq 0, \quad (\text{A10})$$

with equality being achieved when $Z = W$. Figure 20 represents this definition schematically, showing the true χ^2 function and ϕ . The trick of the method is to define ϕ such that it is equal to χ^2 at W , greater than χ^2 everywhere else, and easily minimizable. Then one can use the minimum of ϕ as the update and be guaranteed that one's updates do not increase χ^2 .

The function ϕ can be analytically minimized with respect to its first argument:

$$\phi(W^*, Z) \leq \phi(W, Z) \quad \forall W, Z, \quad (\text{A11})$$

$$W_{ki}^* = Z_{ki} \frac{\sum_n X_{kn} H_{in}}{\sum_{nl} H_{in} H_{ln} Z_{kl}}. \quad (\text{A12})$$

If we set $Z = W$, this becomes exactly equation (A3), and now we can easily prove the validity of this update rule:

$$\chi^2(W) = \phi(W, W) \geq \phi(W^*, W) \geq \chi^2(W^*), \quad (\text{A13})$$

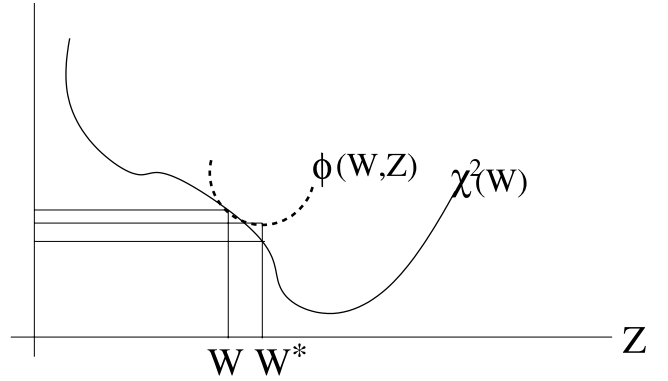


FIG. 20.—Example diagram of the definition of ϕ in the text. Here, χ^2 represents the actual χ^2 , while ϕ is designed such that it exceeds χ^2 except at the single point W . By minimizing ϕ we can find a point W^* that we know to have an equal or better χ^2 than that at W .

where the first inequality comes from the fact that W^* minimizes $\phi(\cdot, W)$ (here and below, a dot indicates “for any matrix”) with respect to its first argument, and the second comes from the fact that $\phi(W^*, \cdot)$ is a bound on $\chi^2(W^*)$. The proof of validity for the update (eq. [A3]) is analogous by symmetry.

To prove the validity of our update (eq. [A6]) for our new problem, we proceed in a similar fashion, using the lemma twice to construct consecutive upper bounds on the cost:

$$\begin{aligned} \chi^2(B) &= \sum_{knls} A_{ki} A_{kl} B_{ij} B_{ls} M_{jn} M_{sn} \\ &\quad - 2 \sum_{knij} X_{kn} A_{ki} B_{ij} M_{jn} + \sum_{kn} X_{kn}^2, \end{aligned} \quad (\text{A14})$$

$$\begin{aligned} \phi(B, Z, \beta) &= \sum_{knls} A_{ki} A_{kl} B_{ij}^2 \frac{Z_{ks} \beta_{lj}}{Z_{kj} \beta_{ij}} M_{jn} M_{sn} \\ &\quad - 2 \sum_{knij} X_{kn} A_{ki} B_{ij} M_{jn} + \sum_{kn} X_{kn}^2, \end{aligned} \quad (\text{A15})$$

$$\phi(B, Z, \beta) \geq \chi^2(B) \quad \forall B_{ij} \geq 0, Z_{kj} \geq 0, \beta_{ij} \geq 0, \quad (\text{A16})$$

with equality being achieved when $Z = AB$ and $\beta = B$.

Once again, the bound ϕ can be analytically minimized with respect to its first argument:

$$\phi(B^*, Z, \beta) \leq \phi(B, Z, \beta) \quad \forall B, Z, \beta, \quad (\text{A17})$$

$$B_{ij}^* = \beta_{ij} \frac{\sum_{kn} X_{kn} A_{ki} M_{jn}}{\sum_{knls} A_{ki} A_{kl} (Z_{ks} \beta_{lj} / Z_{kj}) M_{jn} M_{sn}}. \quad (\text{A18})$$

If we set $Z = AB$ and $\beta = B$, this becomes exactly equation (A8), and we can now prove the validity of this update rule:

$$\chi^2(B) = \phi(B, AB, B) \geq \phi(B^*, AB, B) \geq \chi^2(B^*), \quad (\text{A19})$$

where the first inequality comes from the fact that B^* minimizes $\phi(\cdot, AB, B)$ with respect to its first argument and the second comes from the fact that $\phi(B^*, \cdot, \cdot)$ is a bound on $\chi^2(B^*)$. The only condition we require is that the elements of the matrix MM^\top are all nonnegative.

A3. NONUNIFORM UNCERTAINTIES

When different entries X_{kn} of the data matrix have different uncertainties, the natural objective function is the weighted

TABLE 3
HDUs OF `k_nmf_derived.default.fits`

Number	Name	Dimensions	Description
0.....	templates	$N_{\text{basis}} \times N_t$	Coefficients in basis space for each template
1.....	spec	$N_{\text{spec}} \times N_t$	Smoothed spectrum of each template
2.....	spec_nl	$N_{\text{spec}} \times N_t$	Smoothed spectrum of each template, lines removed
3.....	spec_nd	$N_{\text{spec}} \times N_t$	Smoothed spectrum of each template, without dust
4.....	spec_nl_nd	$N_{\text{spec}} \times N_t$	Smoothed spectrum of each template, without lines or dust
5.....	rawspec	$N_{\text{spec}} \times N_t$	Unsmoothed spectrum of each template
6.....	rawspec_nl	$N_{\text{spec}} \times N_t$	Unsmoothed spectrum of each template, lines removed
7.....	rawspec_nd	$N_{\text{spec}} \times N_t$	Unsmoothed spectrum of each template, without dust
8.....	rawspec_nl_nd	$N_{\text{spec}} \times N_t$	Unsmoothed spectrum of each template, without lines or dust
9.....	lspec	$N_{\text{spec}} \times N_t$	Emission-line spectrum
10.....	extinction	$N_{\text{spec}} \times N_t$	Extinction as a function of wavelength
11.....	lambda	N_{spec}	Wavelength grid (Å)
12.....	sfr	$N_{\text{age}} \times N_t$	Star formation rate ($M_{\odot} \text{ yr}^{-1}$) as a function of time
13.....	metallicity	$N_{\text{age}} \times N_t$	Average metallicity as a function of time
14.....	ages	N_{age}	Age grid (yr)
15.....	dage	N_{age}	Age bin size (yr); $\text{sfr} \times \text{dage} = \text{total star formation in each bin}$
16.....	mass	N_t	Total mass formed in each template
17.....	mremain	N_t	Total current stellar mass in each template
18.....	mets	N_t	Average metallicity of current stars in each template
19.....	m300	N_t	Total stellar mass formed in last 300 Myr in each template
20.....	m1000	N_t	Total stellar mass formed in last 1 Gyr in each template
21.....	basis_ages	$N_{\text{age}} \times N_{\text{mets}} \times N_{\text{dust}}$	Ages of each stellar-population basis vector
22.....	basis_mets	$N_{\text{age}} \times N_{\text{mets}} \times N_{\text{dust}}$	Metallicity of each stellar-population basis vector
23.....	basis_dusts	$N_{\text{age}} \times N_{\text{mets}} \times N_{\text{dust}}$	Dust properties of each stellar-population basis vector
24.....	basis_mremain	$N_{\text{age}} \times N_{\text{mets}} \times N_{\text{dust}}$	Fraction of original stellar mass surviving for each basis vector

NOTE.—All quantities are in floating point (4 byte) precision, except `dusts`, which is an array of structures whose format is described in the text.

approximation error (which also corresponds to the negative log likelihood under a Gaussian noise assumption),

$$\chi^2 = \sum_{kn} \left(\frac{X_{kn} - \sum_i W_{ki} H_{in}}{\sigma_{kn}} \right)^2. \quad (\text{A20})$$

This case can easily be handled since during the update for W the elements of H are fixed and vice versa, and the updates are guaranteed not to increase the cost for any nonnegative matrices. In particular, when updating W , we can rewrite the cost function as

$$\chi^2 = \sum_{kn} \left(\frac{X_{kn}}{\sigma_{kn}} - \sum_i W_{ki} \frac{H_{in}}{\sigma_{kn}} \right)^2, \quad (\text{A21})$$

yielding updates of the form

$$W_{ki} \leftarrow W_{ki} \left(\sum_n \frac{X_{kn} H_{in}}{\sigma_{kn}^2} \right) \left(\sum_{mn} \frac{W_{km} H_{mn} H_{in}}{\sigma_{kn}^2} \right)^{-1}, \quad (\text{A22})$$

and similarly, when updating H , we can rewrite the cost function as

$$\chi^2 = \sum_{kn} \left(\frac{X_{kn}}{\sigma_{kn}} - \sum_i \frac{W_{ki} H_{in}}{\sigma_{kn}} \right)^2, \quad (\text{A23})$$

yielding updates of the form

$$H_{in} \leftarrow H_{in} \left(\sum_k \frac{W_{ki} X_{kn}}{\sigma_{kn}^2} \right) \left(\sum_{mk} \frac{W_{ki} W_{km} H_{mn}}{\sigma_{kn}^2} \right)^{-1}. \quad (\text{A24})$$

This argument can be equally applied to our extended model, yielding the final update equations that are actually implemented in the `kcorrect` code:

$$A_{ki} \leftarrow A_{ki} \left(\sum_{jn} \frac{X_{kn} M_{jn} B_{ij}}{\sigma_{kn}^2} \right) \left(\sum_{mljn} \frac{A_{km} B_{mj} M_{jn} M_{nl} B_{il}}{\sigma_{kn}^2} \right)^{-1}, \quad (\text{A25})$$

$$B_{ij} \leftarrow B_{ij} \left(\sum_{kn} \frac{A_{ki} X_{kn} M_{jn}}{\sigma_{kn}^2} \right) \left(\sum_{mlkn} \frac{A_{ki} A_{km} B_{ml} M_{ln} M_{jn}}{\sigma_{kn}^2} \right)^{-1}. \quad (\text{A26})$$

APPENDIX B

FORMAT FOR TEMPLATES

We have fitted several different sets of templates that we release with the code, which we denote

1. `default`, the default set of five templates;
2. `1rg1`, the single-template fit to LRGs; and
3. `goods`, the five-template fit to just the GOODS data.

The information about the default set of templates is contained in the file `data/templates/k_nmf_derived.default.fits` in the `kcorrect` project. This file has 25 header and data units (HDUs), each listed in Table 3 and described in more detail in the paragraphs below. There are similar files for the `1rg1` and `goods` template sets.

As described in § 2.2, there are $N_{\text{basis}} = 485$ basis spectra, consisting of 450 different instantaneous burst stellar populations ($N_{\text{age}} = 25$ ages, $N_{\text{mets}} = 6$ metallicities, and $N_{\text{dust}} = 3$ dust properties) plus 35 different emission-line models. The `templates` HDU has the coefficients of the five templates in this basis space.

For each of the five templates, we have the template spectrum `spec` in units of $\text{ergs s}^{-1} \text{cm}^{-2} \text{\AA}^{-1} M_{\odot}^{-1}$, as it would be observed at 10 pc distance. The wavelength grid is in the `lambda` HDU. As noted above, the models are smoothed at 300 km s^{-1} resolution; the `rawspec` HDUs have the original (unsmoothed) models from Bruzual & Charlot (2003). In addition, we give versions without the emission lines (with the `_n1` suffix) and without the dust extinction applied (with the `_nd` suffix). The actual emission-line-only spectra for each template are in the `lspec` HDU. Finally, the multiplicative dust extinction factor for each template spectrum is given in the `extinction` HDU.

We include the star formation rate as a function of time in the `sfr` HDU (the age grid used is in the `ages` HDU). The time differential used to quantify this rate is in the `dage` HDU; to get the total number of stars formed at each age, multiply `sfr` by `dage`. The average metallicity of the stars formed as a function of time is in the `metallicity` HDU.

The total mass formed in each template (in solar masses) is in the `mass` HDU; this is actually just unity for each template. The total surviving stellar mass for each template is in the `mremain` HDU.

The metallicity in the surviving stars is given in the `mets` HDU. The total mass in stars formed in the last 300 Myr is in the `m300` HDU, and the total mass formed in the last 1 Gyr is in the `m1000` HDU.

The properties of the 450 stellar-population basis vectors are given in the four HDUs `basis_ages`, `basis_mets`, `basis_dusts`, and `basis_mremain`. Respectively, these give the ages, metallicities, dust properties, and fraction of original stellar mass remaining for each instantaneous burst in the grid. The dust properties are given in terms of a structure with four elements that refer to the properties in the multiple scattering model of Witt & Gordon (2000):

1. GEOMETRY: the geometry of the dust (e.g., “shell”).
2. DUST: the dust extinction curve (e.g., “MW” for Milky Way extinction and “SMC” for Small Magellanic Cloud-type extinction).
3. STRUCTURE: structure of the dust distribution (“h” for homogeneous and “c” for clumpy).
4. TAUVE: the amount of dust (the total optical depth in the V band).

NOTICE

It has been brought to our attention that the reference list was missing in the PDF version of this article at the time of its original publication in 2007. The reference list has always been present in the HTML and is reproduced below.

The Astronomical Journal
September 25, 2012

REFERENCES

- Bell, E. F., & de Jong, R. S. 2001, *ApJ*, 550, 212
Bertin, E., & Arnouts, S. 1996, *A&AS*, 117, 393
Bessell, M. S. 1990, *PASP*, 102, 1181
Blanton, M. R., Lin, H., Lupton, R. H., Maley, F. M., Young, N., Zehavi, I., & Loveday, J. 2003a, *AJ*, 125, 2276
Blanton, M. R., et al. 2003b, *AJ*, 125, 2348
—. 2005, *AJ*, 129, 2562
Brown, T. M., Bowers, C. W., Kimble, R. A., Sweigart, A. V., & Ferguson, H. C. 2000, *ApJ*, 532, 308
Bruzual, G., & Charlot, S. 2003, *MNRAS*, 344, 1000
Chabrier, G. 2003, *PASP*, 115, 763
Cohen, M., Wheaton, W. A., & Megeath, S. T. 2003, *AJ*, 126, 1090
Connolly, A. J., Szalay, A. S., Bershadsky, M. A., Kinney, A. L., & Calzetti, D. 1995, *AJ*, 110, 1071
Davis, M., et al. 2003, *Proc. SPIE*, 4834, 161
Eisenstein, D. J., et al. 2001, *AJ*, 122, 2267
Faber, S. M., et al. 2003, *Proc. SPIE*, 4841, 1657
Fukugita, M., Ichikawa, T., Gunn, J. E., Doi, M., Shimasaku, K., & Schneider, D. P. 1996, *AJ*, 111, 1748
Giavalisco, M., et al. 2004, *ApJ*, 600, L93
Greggio, L., & Renzini, A. 1990, *ApJ*, 364, 35
Hayes, D. S. 1985, in *IAU Symp. 111, Calibration of Fundamental Stellar Quantities*, ed. D. S. Hayes, L. E. Pasinetti, & A. G. Davis Phillip (Dordrecht: Reidel), 225
Hogg, D. W. 1999, in *ASP Conf. Ser. 193, The Hy-Redshift Universe: Galaxy Formation and Evolution at High Redshift*, ed. A. J. Bunker & W. J. M. van Breugel (San Francisco: ASP), 224
Hogg, D. W., Finkbeiner, D. P., Schlegel, D. J., & Gunn, J. E. 2001, *AJ*, 122, 2129
Hogg, D. W., et al. 2002, *AJ*, 124, 646
Hopkins, A. M., et al. 2003, *ApJ*, 599, 971
Jarrett, T. H., Chester, T., Cutri, R., Schneider, S., Skrutskie, M., & Huchra, J. P. 2000, *AJ*, 119, 2498
Kauffmann, G., et al. 2003, *MNRAS*, 341, 33
Kennicutt, R. C., Jr., Tamblyn, P., & Congdon, C. E. 1994, *ApJ*, 435, 22
Kewley, L. J., Dopita, M. A., Sutherland, R. S., Heisler, C. A., & Trevena, J. 2001, *ApJ*, 556, 121
Kurucz, R. L. 1991, in *Precision Photometry: Astrophysics of the Galaxy*, ed. A. G. Davis Philip, A. R. Upgren, & K. A. Janes (Schenectady: Davis), 27
Lee, D. D., & Seung, H. S. 1999, *Nature*, 401, 788
—. 2000, *Adv. Neural Inf. Processing Syst.*, 556
Lupton, R. H., Gunn, J. E., Ivezić, Ž., Knapp, G. R., Kent, S., & Yasuda, N. 2001, in *ASP Conf. Ser. 238, Astronomical Data Analysis Software and Systems X*, ed. F. R. Harnden, Jr., F. A. Primini, & H. E. Payne (San Francisco: ASP), 269
Maraston, C. 2005, *MNRAS*, 362, 799
Martin, D. C., et al. 2005, *ApJ*, 619, L1
Oke, J. B., & Sandage, A. 1968, *ApJ*, 154, 21
Pier, J. R., Munn, J. A., Hindsley, R. B., Hennessy, G. S., Kent, S. M., Lupton, R. H., & Ivezić, Ž. 2003, *AJ*, 125, 1559
Richards, G., et al. 2002, *AJ*, 123, 2945
Schneider, D. P., Gunn, J. E., & Hoessel, J. G. 1983, *ApJ*, 264, 337
Sha, F., Saul, L., & Lee, D. 2002, *Tech. Rep. MS-CIS-02-19* (Philadelphia: Univ. Pennsylvania)
Skrutskie, M. F., et al. 1997, in *The Impact of Large Scale Near-IR Sky Surveys*, ed. F. Garzon et al. (Dordrecht: Kluwer), 25
Smith, J. A., et al. 2002, *AJ*, 123, 2121
Stoughton, C., et al. 2002, *AJ*, 123, 485
Strauss, M. A., et al. 2002, *AJ*, 124, 1810
Vassiliadis, E., & Wood, P. R. 1993, *ApJ*, 413, 641
Witt, A. N., & Gordon, K. D. 2000, *ApJ*, 528, 799
York, D., et al. 2000, *AJ*, 120, 1579